Alleviation of Cocaine Withdrawal and Pertinent Interactions between Salvinorin-based Antagonists and Kappa Opioid Receptor

Nicholas S. Akins,[1] Salahuddin F. Mohammed,[1] Pankaj Pandey,[2] Seong Jong Kim,[3] Fahri Mahdi,[1] Md Imdadul H. Khan,[1] Emaya Moss,[1] Charlie J. Worth,[1] Madeline M. Keanne,[1] Amar G. Chittiboyina,[2] Robert J. Doerksen,[1] Jason J. Paris,[1] Hoang V. Le[1,]*

[1]Department of BioMolecular Sciences and Research Institute of Pharmaceutical Sciences, School of Pharmacy, University of Mississippi, University, MS 38677, U.S.A

[2]National Center for Natural Products Research and Research Institute of Pharmaceutical Sciences, University of Mississippi, University, MS 38677, U.S.A

[3]Natural Products Utilization Research Unit, United States Department of Agriculture, Agricultural Research Service, University, MS 38677, U.S.A

ABSTRACT: The kappa opioid receptor (KOR) is involved in the regulation of both reward and mood processes. Recent reports find that the use of drugs of abuse increases the production of dynorphin and overall activation of KOR. Long-acting KOR antagonists, such as norbinaltorphimine (nor-BNI), JDTic, and 5'-guanidinonaltrindole (GNTI), are shown to halt depressive and anxiety-related disorders, which are the common side effects of withdrawal that can lead to the relapse of drug use. Unfortunately, these prototypical KOR antagonists are known to induce selective KOR antagonism that is delayed by hours and extremely prolonged, and their use in humans comes with serious safety concerns because they possess a large window for potential drug-drug interactions. Additionally, their persisted pharmacodynamic activities can hinder the ability to reverse unanticipated side effects instantly. Herein we report our studies on the lead selective, salvinorin-based KOR antagonist (**1**) as well as nor-BNI on C57BL/6N mice for spontaneous cocaine withdrawal. Assessment of pharmacokinetics showed **1** to be a short-acting compound with an average half-life of 3.75 h across different compartments (brain, spinal cord, liver, and plasma). Both **1** (5 mg/kg) and nor-BNI (5 mg/kg) were shown to reduce spontaneous withdrawal behavior in mice, with **1** producing additional anti-anxiety-like behavior in a light-dark transition test (however, no mood-related effects of **1** or nor-BNI were observed at the current dosing in an elevated plus maze or a tail suspension test). Our results support the study of selective, short-acting KOR antagonists for the treatment of psychostimulant withdrawal and the associated negative mood states that contribute to relapse. Additionally, we identified pertinent interactions between **1** and KOR via computational studies, including induced-fit docking, mutagenesis, and molecular dynamics simulations, to gain insights into the design of future selective, potent, and short-acting salvinorin-based antagonists.

Key words: Kappa opioid receptor, short-acting antagonists, salvinorin compounds, cocaine withdrawal, mental health disorders

1. INTRODUCTION

The current drug crises in America are predominantly focused on opioids. However, cocaine overdose is increasing exponentially in the U.S.[1–4] From 2018 to 2019, cocaine overdose deaths increased by nearly 9%.[5] In 2019, cocaine was responsible for 16,000 American deaths (19% of all overdose deaths in the United States).[5] In 2020, over 5 million Americans (almost 2% of the population) reported current cocaine use.[6] There are no current FDA-approved treatments for cocaine use disorders. Unlike the case of opioid/heroin use disorder, which has some therapeutic recourse (albeit, limited),[7–9] cognitive behavioral therapy is the only effective clinical option for cocaine abuse.[10,11] Research on cocaine dependence has been widely carried out, but has yet to yield efficacious medications.[12] A cocaine epidemic is imminent; thus, the need for novel therapeutics for cocaine use disorder is urgent.[13]

Preclinical models have demonstrated the kappa opioid receptor (KOR) to be a central player in the regulation of both reward and mood processes.[14,15] KOR contributes to the regulation of the dopamine mesolimbic pathway, which is composed of dopaminergic neurons from the

midbrain ventral tegmental area (VTA) that project to forebrain limbic structures, including the ventral striatum [or nucleus accumbens (NAc)] and prefrontal cortex (PFC) (**Figure 1**).[15] Rewarding properties of drugs of abuse, natural stimuli, and neurobiological effects of stressful experiences strongly interact at the level of KOR signaling. Studies have shown that the use of drugs of abuse increases the production of dynorphin and overall activation of KOR.[16] In a recent study, co-administration of buprenorphine and naltrexone, which produced the effects of a pure KOR antagonist, resulted in an improvement in the outcome of opioid dependence in terms of treatment retention, negative urinalyses, reduced dysphoria, improved mood, and reduced craving.[17] Another study showed that blocking KOR within the VTA prior to forced-swim stress in mice prevented the reinstatement of cocaine-seeking.[18] KOR antagonism was also recently shown to reverse heroin withdrawal-induced hyperalgesia in male and female rats.[19] These results suggested that antagonizing KOR may halt some depressive and anxiety-related symptoms that are associated with withdrawal, along with motivational withdrawal symptoms, to ultimately reduce drug use relapse.

Long-acting KOR antagonists, such as norbinaltorphimine (nor-BNI), JDTic, and 5'-guanidinonaltrindole (GNTI), have been used as prototypical therapeutic agents for various neuropsychiatric conditions, including depression, anxiety, and substance abuse disorders.[15,20–23] Unfortunately, these prototypical KOR antagonists are known to induce selective KOR antagonism that is delayed by hours and extremely prolonged. A study in mice showed that the brain uptakes of these compounds were very slow and their presence in the brain was persistent and still detectable at one week.[20] Their pharmacodynamic activities can persist long after the compounds were eliminated from the body. A single injection of nor-BNI in humans can block the effects of KOR agonists for a couple of months.[15,24] Thus, while these long-acting KOR antagonists do not chemically alter KOR, they are often considered to be KOR inactivators due to their long-term effects. The use of these receptor-inactivating KOR antagonists in humans comes

with serious safety concerns because they possess a large window for potential drug-drug interactions.[15] These compounds also promote desensitization in drug abuse treatment, potentially promoting tolerance, and complicate preclinical assessments in paradigms that require multiple administrations (such as self-administration). Additionally, their persisted pharmacodynamic activities can hinder the ability to reverse unanticipated side effects instantly; thus, these receptor-inactivating KOR antagonists may lead to detriment results when serious side effects occur. JDTic, for example, advanced to phase I human clinical trials for the treatment of cocaine abuse,[23] but its development was halted due to adverse events such as ventricular tachycardia that could not be reversed instantly.[22] The reasons for the extraordinarily long time-course of those KOR antagonists are yet to be understood.
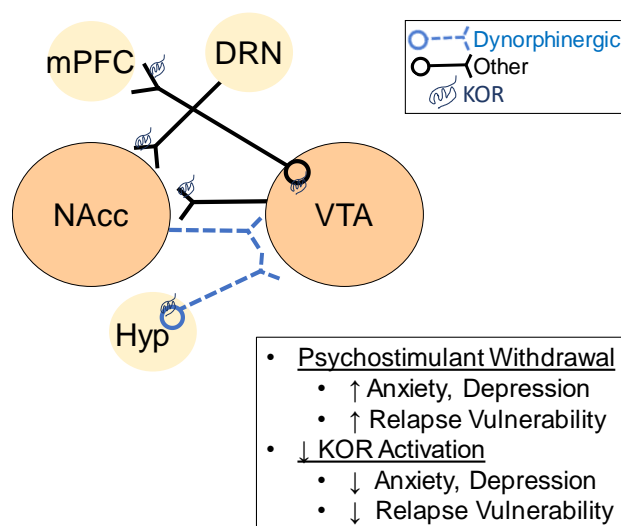

Figure 1. Dynorphin-KOR Modulation Inherent to CNS Reward Circuitry. A simplified scheme of neuronal circuits implicated in the dynorphinergic regulation of reward, which are modulated by both dynorphins (released from dotted projections in blue) and via the kappa opioid receptor (KOR)[14] in nucleus accumbens (NAcc), ventral tegmental area (VTA), medial prefrontal cortex (mPFC), dorsal raphe nucleus (DRN), and hypothalamus (Hyp). Inhibiting KOR is hypothesized to reduce anxiety/depression associated with stimulant withdrawal, thus reducing the vulnerability to relapse.

KOR antagonists that are shorter-acting than nor-BNI, JDTic, GNTI are currently being developed and studied as they possess more

favorable drug profiles. These compounds, such as CERC-501 (a.k.a. aticaprant), PF-4455242, and AZ-MTAB, have already shown promising results for depression and substance use disorders in preclinical models.[15,25] For example, CERC-501 has a biological half-life in humans (plasma) of 38.5 hours[15] and reversed the analgesic effects induced by U-69593, a potent KOR agonist, for up to a week.[22] It advanced to phase II clinical trials as an augmentation to antidepressant therapy for treatment-resistant depression; unfortunately, the clinical trials were later terminated due to slow enrollment.[26]

Salvinorin A is the main active ingredient of the hallucinogenic plant *Salvia divinorum* that has been safely used by the Mazatec people for centuries in religious rituals.[27] It is one of the most potent, naturally occurring opioid agonists, with high selectivity and affinity for KOR. It has the potential to be beneficial in treatment therapies of various central nervous system (CNS) disorders. atai Life Sciences is currently planning to develop salvinorin A for treatment-resistant depression, substance use disorder, and pain, with clinical trials expected to begin in the second half of 2022.[28] Additionally, salvinorin A has been used as an important prototype for the development of related drug candidates.[29–39] Notably, there are only six salvinorin-based compounds in the literature that have demonstrated antagonism against any of the opioid receptors (**1–6**, **Figure 2**);[39] all other reported salvinorin-based compounds are agonists. Compounds **1–5** are antagonists at KOR, μ-opioid receptor (MOR), and δ-opioid receptor (DOR), with **1** being the most selective for KOR.[39] Meanwhile, compound **6** is an antagonist at MOR and DOR, but a partial agonist at KOR.[39]
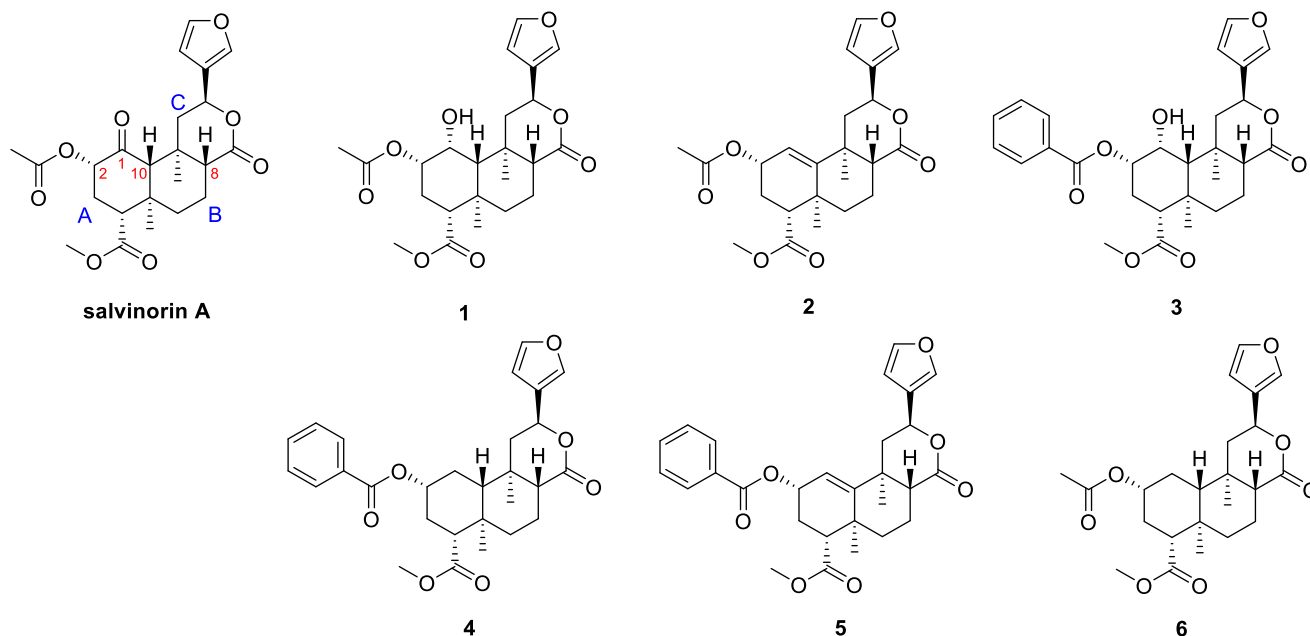

Figure 2. Structures of salvinorin A and known salvinorin-based opioid receptor antagonists **1–6**

The common feature among these opioid receptor antagonists is a small structural modification at C1, the replacement of the ketone with an alcohol, alkene, or methylene functional group. We recognized that although the structural modification at C1 was small, it resulted in a significant change to the overall layout of the tricyclic rings of the salvinorin scaffold, which in turn produced major differences in functional activities towards the opioid receptors. No salvinorin antagonists have ever been evaluated *in vivo*. Based on previous studies that showed salvinorin C2-esters being short-acting (due to the fast hydrolysis of the ester group), we intended to use the most selective KOR antagonist (**1**) as a proof-of-concept. Herein we report our studies of

compound **1** as well as nor-BNI on C57BL/6N mice for spontaneous cocaine withdrawal. We also assessed pharmacokinetics (PK), compartment distribution, and carried out computational studies to identify pertinent interactions between **1** and KOR to gain insights into the design of future selective, potent, and short-acting salvinorin-based KOR antagonists.

2. RESULTS AND DISCUSSION

2.1 Synthesis of 1

We started the synthesis of **1** by reducing the C1 ketone in salvinorin A to alcohol using $NaBH_4$. Deacetylation at C2 and epimerization at C8 occurred during this reaction.[39,40] The deacetylated diol **7a** was obtained in a 57% yield (**Scheme 1**). The C8-epimer of **7a** (which is **7b**) was obtained in a 40% yield. Reacetylation at C2 of **7a** using acetic anhydride in pyridine at room temperature provided the desired product, compound **1**, in a 91% yield. Overall, **1** was obtained in a 52% yield after 2 steps.
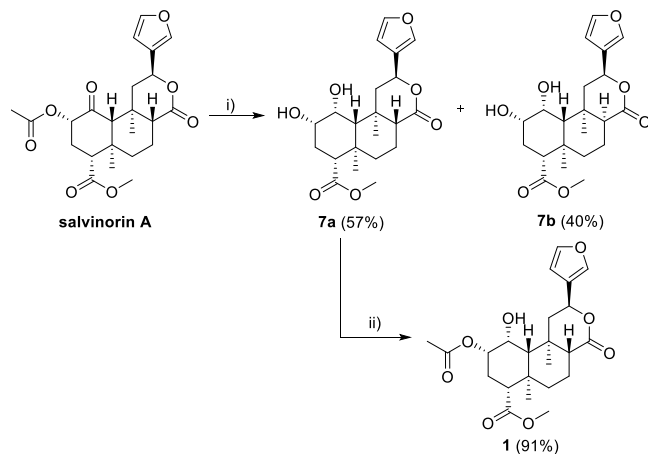
Reagents and conditions: i) $NaBH_4$, EtOH, 50°C, 1h; **ii)** Ac_2O, py, rt, 5h
Abbreviations: $NaBH_4$, sodium borohydride; EtOH, ethanol; Ac_2O, acetic anhydride; py, pyridine

Scheme 1. Synthetic route for compound **1**

2.2 Pharmacokinetics studies of 1

To assess the time course of metabolism and distribution of **1**, PK studies were carried out. A single i.p. dose of **1** (5 mg/kg) was injected into C57BL/6N mice (n=3/group), and their brain, dorsal spinal cord, liver, and plasma were collected at 5, 15, 30, 60, 120, and 360 min post-

injection. Circulating, central, and liver contents were assessed via LC-MS/MS. Based on the concentration vs. time curves (**Figures 3A–D**), we project **1** to be present in the brain for up to ~26–31 h, spinal cord ~19–22 h, liver ~13–15 h, and plasma ~18–22 h. The half-life of **1** in the brain (5.2 h) was longer than in other biological matrices (spinal cord 3.7 h, liver 2.5 h, plasma 3.6 h). The apparent T_{max} (the time that the maximum concentration of **1** was observed) occurred at 30 min in the brain, spinal cord, and plasma, and at 60 min in the liver. Compound **1** exhibited the shortest half-life but highest T_{max} in the liver. These values suggested that **1** may be metabolized in the liver and excreted biliarily, similar to salvinorin A.[41] The Ri_{AUC} (calculating experimental matrix to plasma partition coefficient of **1**) was 0.9~1.0.[42] Overall, our results indicate **1** to be the first short-acting, salvinorin-based KOR antagonist.

2.3 Evaluation of 1 on spontaneous motor, anxiety-like, and depression-like behaviors associated with cocaine withdrawal

To assess the effects of compound **1** on the motoric and affective withdrawal associated with cocaine, C57BL/6N mice (n=7–13/group) were administered saline or an escalating regimen of cocaine over three days (5, 10, and 20 mg/kg). This dosing range produces psychostimulation in mice and sensitization when administered sequentially.[40,41] On the final day, mice were co-administered vehicle, nor-BNI, or compound **1** (both 5 mg/kg; **Figure 4**). Mice were allowed to undergo 48 h of withdrawal.

A previous study has shown that spontaneous motor behaviors are indicative of cocaine withdrawal;[43] therefore, we first assessed the motor phenotype of mice that had received saline or escalating cocaine dosing in an open field test. The results showed that cocaine exposure significantly influenced the distance [$F(5,48) = 4.93$, $p < 0.05$] (**Figure 5A**), speed of travel [$F(5,48) = 4.87$, $p < 0.05$] (**Figure 5B**), and the number of rears made by mice in an open field [$F(5,48) = 3.44$, $p < 0.05$] (**Figure 5C**). Consistent with the behaviors of cocaine withdrawal, mice in the cocaine-exposed control group traveled significantly greater distances ($p =$

0.003; **Figure 5A**) at greater velocities ($p = 0.004$; **Figure 5B**), and demonstrated more frequent rearing behavior ($p = 0.02$; **Figure 5C**) than did saline-administered controls. Post-treatment with either the receptor-inactivating KOR antagonist, nor-BNI ($p = 0.004$–0.005), or the short-acting KOR antagonist, **1** ($p = 0.001$–0.02), significantly attenuated cocaine-mediated spontaneous motor behaviors (**Figures 5A–C**). No significant differences were observed in the time spent rearing (**Table 1**).

We additionally assessed the effects of nor-BNI and **1** on anxiety- and depression-like behavior in response to saline or escalated cocaine withdrawal. In a light-dark transition test, the short-acting KOR antagonist, **1**, was shown to significantly influence the anxiety-like behaviors [$F(5,48) = 2.69$, $p < 0.05$] (**Table 1**). Administration of **1** immediately following the last dose of saline or cocaine significantly increased the latency to cross into the dark chamber indicating a reduction in anxiety-like behavior when compared to saline-administered controls ($p = 0.007$–0.04), those administered escalated cocaine ($p = 0.006$-0.04), or those administered saline/nor-BNI ($p = 0.04$). Cocaine exposure increased compartment transitions in this test [$F(5,48) = 3.40$, $p < 0.05$], indicating

increased motor behavior ($p = 0.048$) and nor-BNI significantly attenuated this effect ($p = 0.03$; **Table 1**). Significant differences were not observed in the time spent in the light or dark chambers (**Table 1**). Similarly, no differences were observed in the amount of time spent on the open or closed arms of an elevated plus maze; albeit, nor-BNI did increase the total arm entries when combined with cocaine [$F(5,48) = 2.76$, $p < 0.05$] (**Table 1**). Significant differences were not observed in the amount of time spent immobile in the tail suspension test (**Table 1**).

We also assessed the effects of **1** on psychomotor behavior when cocaine was on-board. No effects of **1** were seen when it was assessed for its capacity to reduce the rewarding and psychostimulatory capacity of cocaine in a conditioned place preference paradigm (**Figure S1**).

Overall, our evaluation of **1** on spontaneous motor, anxiety-like, and depression-like behaviors associated with cocaine withdrawal has shown that **1** reduced the motoric and affective complications of cocaine withdrawal. These primary therapeutic actions of **1** may be due to its longer residence in the brain than in other compartments.
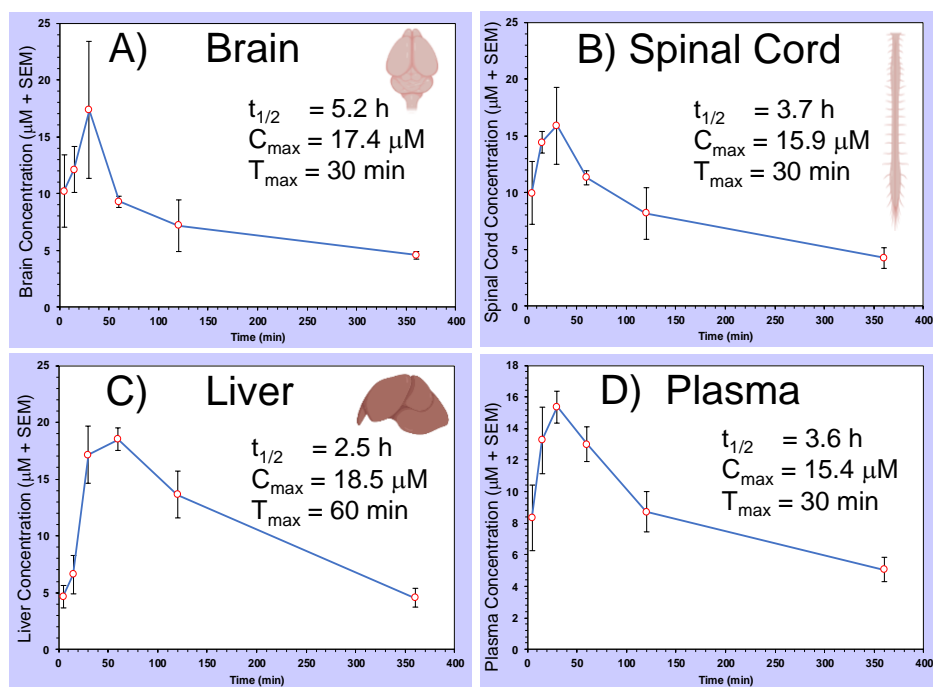

Figure 3. PK properties of compound **1** including half-life ($t_{1/2}$), max. concentration (C_{max}), and time to C_{max} (T_{max}) in (**A**) brain, (**B**) spinal cord, (**C**) liver, and (**D**) plasma (n=3 independent observations per timepoint)
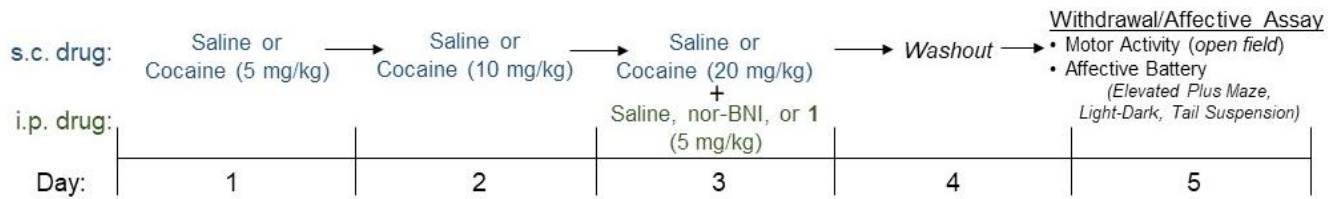
Figure 4. Dosing schedule and timeline for motor and affective withdrawal assays
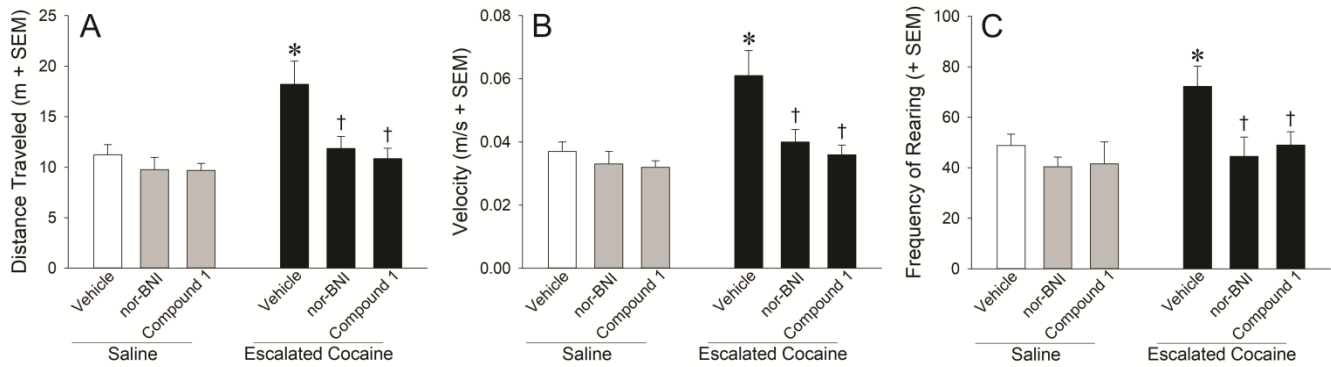

Figure 5. Mice (n=7-13) were administered saline or an escalating regimen of cocaine with nor-BNI (5 mg/kg) or **1** (5 mg/kg) as depicted in the Figure 3 timeline. 48 h after the cessation of cocaine, all mice were assessed in an open field for the (A) distance and (B) velocity traveled, and (C) the frequency of rearing. * significantly differs from saline/vehicle control. † significantly differs from cocaine/vehicle-treatment, $p < 0.05$.

Table 1. Motor and affective behavioral measures. *significantly differs from saline/vehicle; †significantly differs from escalated cocaine/vehicle; ‡significantly differs from saline/nor-BNI, $p < 0.05$.

	Saline			Escalated Cocaine		
	Vehicle (n=7)	nor-BNI (n=8)	**1** (n=8)	Vehicle (n=13)	nor-BNI (n=9)	**1** (n=9)
Open Field						
Time Spent Rearing (s)	54 ± 15	49 ± 13	56 ± 18	70 ± 12	49 ± 18	65 ± 18
Elevated Plus Maze						
Open Arm Time (s)	26 ± 5	34 ± 6	24 ± 6	45 ± 15	41 ± 7	26 ± 9
Closed Arm Time (s)	250 ± 7	248 ± 8	259 ± 10	225 ± 16	228 ± 11	254 ± 7
Total Arm Entries	15 ± 1	20 ± 2	15 ± 2	21 ± 3	25 ± 2	16 ± 2
Light-Dark Transition						
Latency to Dark (s)	4 ± 1	18 ± 12	58 ± 18*†‡	10 ± 3	24 ± 11	44 ± 21*†
Number of Transitions	15 ± 3	15 ± 3	9 ± 2	23 ± 3	15 ± 3*	19 ± 2
Light Zone Time (s)	48 ± 8	82 ± 17	84 ± 20	82 ± 16	65 ± 22	114 ± 24
Dark Zone Time (s)	246 ± 9	217 ± 17	216 ± 20	214 ± 15	224 ± 23	186 ± 24
Tail Suspension						
Time Immobile (s)	172 ± 12	163 ± 14	177 ± 11	166 ± 8	178 ± 10	164 ± 5

2.4 Docking and Computational Site-directed Mutagenesis on KOR, MOR, and DOR

In the two-state receptor model, a full agonist binds only to the active state of the G protein-coupled receptors (GPCRs), whereas an antagonist binds equally well to both the active and inactive states.[44] The aspartic acid residue on the third helix of all aminergic GPCRs, $D^{3.32}$, plays a significant role in the binding of protonated compounds.[45] Specifically, in the case of opioid receptors, before the discovery of the molecular target of salvinorin A, it was hypothesized that a basic amine on the ligand structure was required for the binding to the opioid receptors. This was due to the basic amine in the structures of all known opioid ligands at that time, such as fentanyl and morphine derivatives.[45] When KOR was identified as the molecular target of salvinorin A, the aforementioned hypothesis was contested as salvinorin A is non-nitrogenous.[45] Interestingly, with other small molecules, mutagenesis and computational studies indicated that an extended hydrogen bond network between the conserved aspartic acid residue on the third helix of KOR, $D138^{3.32}$, and water may exist. Although, in the case of salvinorin A, this interaction is suboptimal, and mutation (D138A) lowered the desolvation cost thus increasing binding affinity to KOR.[46] Since the cocrystal structure of KOR and salvinorin A has not been obtained, many researchers have hypothesized the putative binding modes of salvinorin A to KOR.[46-48] Via *in vitro* mutagenesis and computational studies, the initial recognition pose of salvinorin A in the inactive-state X-ray crystal structure of KOR (PDB: 4DJH)[48] and the putative binding mode of salvinorin A in the active-state X-ray crystal structure of KOR (PDB: 6B73) were proposed.[49] To the best of our knowledge, similar studies for salvinorin-based KOR antagonists have not been carried out.

To study the pertinent interactions between salvinorin-based antagonists and KOR, we docked compounds **1**, **2**, **6**, and salvinorin A into both the active-state (PDB: 6B73) and inactive-state (PDB: 4DJH) X-ray crystal structures of KOR using Glide. Although our work was mainly focused on compound **1**, we also carried out the computational studies for compounds **2** (also a KOR antagonist, but less potent than **1**) and **6** (a partial KOR agonist) to understand the impact of small variations in the structure at C1 and C10 on the selectivity and functionality of the compounds towards KOR. The importance of each ligand-protein interaction between **1** and **2** to KOR was inferred from computational site-directed mutagenesis and successive energy measurements using Prime MM-GBSA in Maestro.[50-52] Our results showed that salvinorin A, **1**, and **2** displayed similar docking poses and GlideScores in the active state of KOR. While the C1 ketone of salvinorin A showed a hydrogen bonding interaction with $Q115^{2.60}$ and the C1 hydroxyl of **1** displayed a hydrogen bonding interaction with $D138^{3.32}$, **2** did not show any hydrogen bonding interaction to the residues in that area (**Figure 6A** and **Table S2**). Our docking results also predicted the binding interactions between salvinorin A and the active state of KOR (to $Y139^{3.33}$, $C210^{ECL2}$, and $Y312^{7.35}$) were similar to the previously reported results by the Roth group[49] (**Figure 6B**).

Our docking of salvinorin A in the inactive state of KOR resulted in a binding mode that matched with the previously reported one done by Roth and coworkers (**Figure 6C**).[46] This binding mode of salvinorin A has been suggested to be the recognition pose of salvinorin A into KOR before the activation of the receptor and rearrangement of itself into the binding mode in the active state.[46] Meanwhile **1** and **2** displayed similar binding modes in both the active state and the inactive state of KOR, reflecting their nature of equal binding as antagonists to both the active and inactive states of KOR (**Figure 6D**). A D138A computational mutation of $D^{3.32}$ resulted in a total loss of the original predicted binding modes for both **1** and **2** within the inactive state of KOR. We suspected that the smaller size of alanine in comparison to aspartic acid led to this alteration (**Table S3**). To further support our assumption, another mutation (D138L) was completed. This mutation revealed a similar binding mode as compared to the wildtype, and it experienced no loss in GlideScore or predicted binding affinity (**Table S3**). We recognized that changing from D to A, or D to L, also came with a change in the polarity besides size. However, the fact that **2**

(which did not show any hydrogen bonding interaction to the residues in that area, as mentioned above) did not change its binding

mode in the mutation compared to the wildtype led us to believe that size in this area is more important for binding affinity.
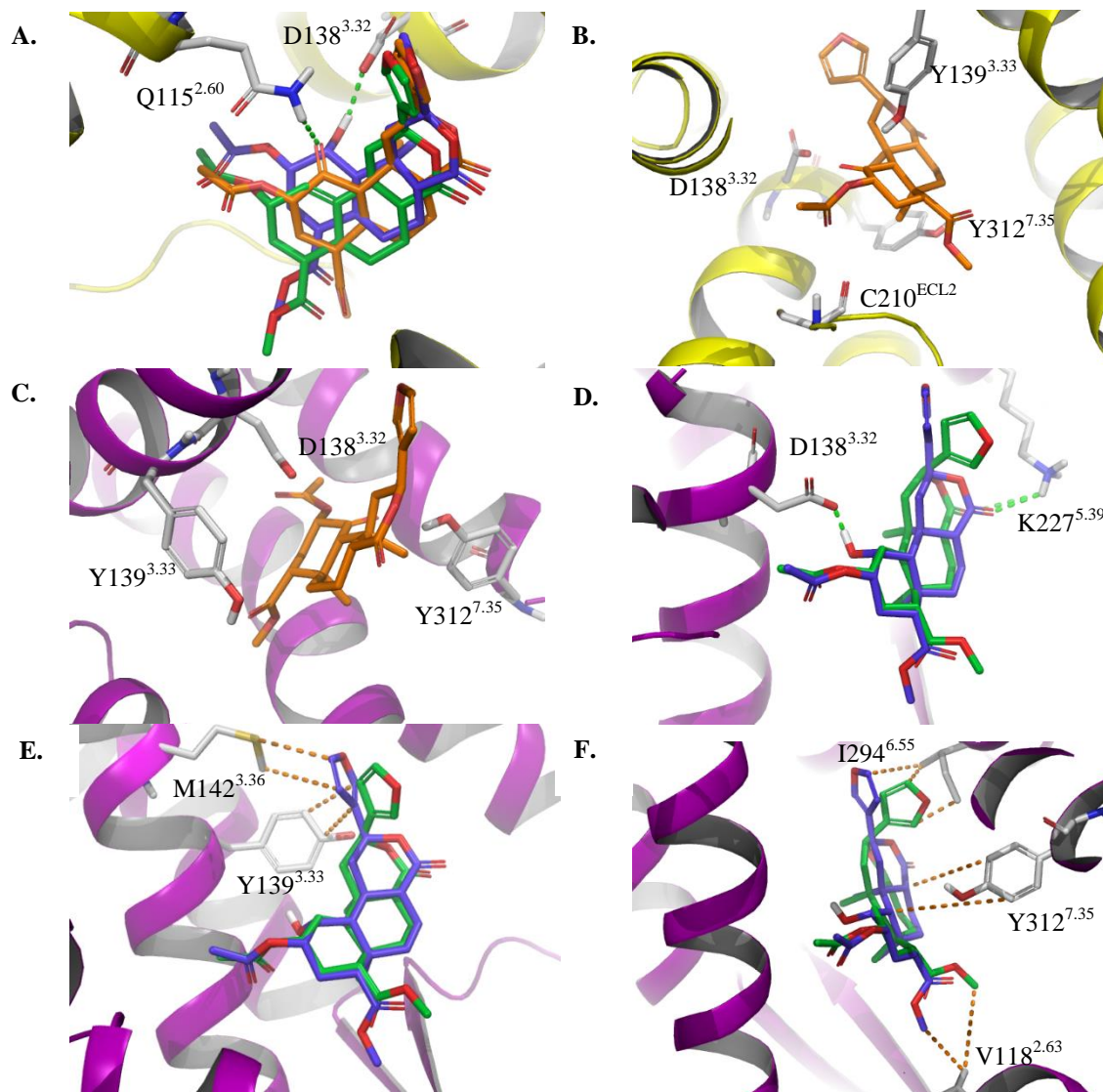

Figure 6. A) Overlay of the binding modes of **1**, **2**, and salvinorin A in the active state of KOR; **B)** Salvinorin A within the active state of the KOR; **C)** Salvinorin A within the inactive state of KOR; **D)** Hydrogen bonding interactions of **1** and **2** with D138 and K227 within the inactive state of KOR; **E)** Hydrophobic interactions of **1** and **2** with Y139 and M142 in the inactive state of KOR; **F)** Hydrophobic interactions of **1** and **2** with I294, Y312, and V118 in the inactive state of KOR. Compound **1** is in blue; **2** is in green; the active state of KOR (PDB: 6B73) is in yellow cartoon; the inactive state of KOR (PDB: 4DJH) is in purple cartoon; hydrogen bonding interactions are depicted as green dashes; and hydrophobic interactions are depicted as orange dashes.

Both **1** and **2** exhibited a strong hydrogen bonding interaction with K227[5.52] and hydrophobic interactions with Y139[3.43] and M142[3.46] in the inactive state of KOR (**Figures 6D–E**). These three residues have been known to be important for the function of KOR.[46] A K227A mutation of K227[5.52] resulted in a decrease in the predicted binding affinity to the inactive state of

KOR for both **1** and **2** (**Table S3**). Meanwhile, a Y139A mutation of Y139[3.43] and an M142A mutation of M142[3.46] resulted in a decrease in the predicted binding affinity to the inactive state of KOR for **1**, but not for **2** (**Table S3**). Notably, **1** and **2** also displayed hydrophobic interactions with I294[6.55], Y312[7.35], V118[2.63] in the inactive state of KOR, three of the four residues that were

previously recognized as important for the selectivity to KOR (V108$^{2.53}$ is the other residue)[46] (**Figure 6F**).

Insights into the binding to KOR:

Similar docking and computational mutagenesis studies were carried out for **1**, **2**, and **6** in the inactive states of MOR (PDB: 4DKL) and DOR (PDB: 4N6H) (**Tables S4–7** and **Figures S2–5**). Our results reinforced the aforementioned importance of I294$^{6.55}$, Y312$^{7.35}$, and V118$^{2.63}$ for the selectivity of ligands, such as **1**, to KOR.

While V$^{2.63}$ and Y$^{7.35}$ were observed to interact well with **1** in KOR, the corresponding N$^{2.63}$ and K$^{2.63}$ (of V$^{2.63}$), and W$^{7.35}$ and L$^{7.35}$ (of Y$^{7.35}$) in MOR and DOR, respectively, did not show any interactions with **1**. Meanwhile, **2** and **6** possessed alternate binding modes and different interactions within MOR and DOR (**Figure S2**). As mentioned earlier, D138$^{3.32}$ does not play a role in salvinorin A's affinity or functional (agonistic) activity towards KOR. Compound **1** (also non-nitrogenous), however, was observed to have hydrogen bonding interaction with D138$^{3.32}$ in KOR, D147$^{3.32}$ in MOR, and D128$^{3.32}$ in DOR (**Figure S3**). Therefore, our results have further suggested that the selectivity of salvinorin-based compounds to KOR, such as **1**, did not likely involve D138$^{3.32}$, but rather all other aforementioned residues, such as I$^{6.55}$, V$^{2.63}$, Y$^{7.35}$.

A previous study done by Roth and coworkers suggested that non-charged ligands, such as salvinorin A, were highly sensitive to mutation within the binding pocket.[46] As mentioned earlier, this study identified the recognition pose of salvinorin A in the inactive state of KOR before the activation of the receptor and rearrangement of itself into the binding mode in the active state. This study also carried out *in vitro* site-directed mutagenesis for Q115$^{2.60}$, I116$^{2.61}$, V118$^{2.63}$, Y139$^{3.33}$, Y312$^{7.35}$, Y313$^{7.36}$, and Y320$^{7.42}$, and suggested that they all resulted in a reduction of the affinity or potency of salvinorin A to KOR.[46] Y139$^{3.33}$, M142$^{3.36}$, K227$^{5.52}$, H291$^{6.52}$, and Y320$^{7.42}$ were shown to specifically affect KOR activation through modulation of P238$^{5.50}$, I146$^{3.40}$, and F283$^{6.44}$.[46] In addition, small rotameric change of the PIF motif, which connects the transmembrane helix 3 (TM3), transmembrane helix 5 (TM5), and transmembrane helix 6 (TM6), upon ligand binding led to a large-scale movement of these helices during activation.[46] Our docking data have suggested that the binding of a salvinorin-based KOR antagonist would alter the rotameric change of this PIF motif, blocking the large-scale movement of these helices, thus preventing the activation of the receptor.

As mentioned earlier, compounds **1** and **2** exhibited similar predicted binding modes in the active and inactive states of KOR, reflecting their nature of equal binding as antagonists to both the active and inactive states. Compound **1** exhibited a hydrogen-bonding interaction between C1-hydroxyl and D138$^{3.32}$ and hydrophobic interactions between C4-ester and V118$^{2.63}$, rings C and D and I294$^{6.55}$, ring A and Y312$^{7.35}$, and C2 acetoxy and Y320$^{7.42}$. Meanwhile, compound **2** (not having the C1-hydroxyl) possessed similar hydrophobic interactions but lacked the hydrogen bonding interaction with D138$^{3.32}$. Therefore, we hypothesized that the hydrogen bonding interaction between C1-hydroxyl of **1** and D$^{3.32}$ helped anchor **1** into its putative binding mode and improve the interactions that are known to aid in the binding, selectivity, and antagonistic functionality to KOR.

Insights into the binding to MOR:

Studies have shown that ligands that bind to MOR would commonly interact with two crucial residues D147$^{3.32}$ and Y148$^{3.33}$, and that antagonists generally display more polar interactions with residues such as Q124$^{2.60}$, Y128$^{2.64}$, N150$^{3.35}$, K233$^{5.40}$, E229$^{3.35}$, and W318$^{7.35}$ than do agonists.[53] As previously reported by the Prisinzano lab, **2** and **6** exhibited higher binding affinities to MOR than that of **1** (K_i values for **1**, **2**, and **6** are 2300, 200, and 170 nM, respectively;[39] the authors reported these as K_e values, but we believe they meant K_i values–the dissociation constant in the inhibition of agonist-stimulated [^{35}S]GTP-γ-S binding assay; K_e is reserved for the elimination constant of a drug, usually from an animal or person). Therefore, we completed similar docking and computational site-directed mutagenesis studies on MOR (as we did on KOR) with these salvinorin-based antagonists to identify the residues that are

important for the selectivity and functionality to this receptor. The results indicated that **1**, **2**, and **6** displayed similar binding modes in MOR (**Figure S2, Tables S4–5**). Small differences among these binding modes were observed, most likely due to the C1-hydroxyl group on **1** exhibiting hydrogen bonding interaction with D147$^{3.32}$ while **2** and **6** did not (**Figures S4B–D**). Compound **2** exhibited hydrogen bonding with Y148$^{3.33}$, K233$^{5.58}$, and W318$^{7.35}$, as well as hydrophobic interactions with other residues (**Figure S4C**). Compound **6** exhibited hydrogen bonding with K233$^{5.58}$ and W318$^{7.35}$, as well as π-stacking interactions with Y326$^{7.42}$ and W293$^{6.48}$ (**Figure S4D**). The results suggested that these additional hydrogen bonding and hydrophobic interactions may be responsible for the higher binding affinities of **2** and **6** to MOR, compared to **1**.

We then carried out computational site-directed mutagenesis studies to determine the importance of these polar and non-polar interactions in the binding of **1**, **2**, and **6** to MOR (**Tables S4–5**). A K233A mutation resulted in a precipitous loss in predicted binding affinities of **2** and **6**, whereas that of **1** was minimally affected (**Table S5**). Meanwhile, a Y147A mutation also lowered predicted binding affinities of **1**, **2**, and **6**, but the effects were not as drastic as that of K233A mutation (**Table S5**). These results suggested that the interaction with Y147$^{3.33}$ in MOR may contribute to the functionality of the ligands in MOR but would have a limited effect on their binding affinities. Furthermore, a W318G mutation resulted in a loss of expected binding affinities for all three compounds (the loss of binding affinity for **2** was greater than that for **6**, which was greater than that for **1**) (**Table S5**). As mentioned earlier, **1** possessed additional hydrogen-bonding interactions with D147$^{3.32}$ and K233$^{5.58}$ that **2** did not have, and **6** displayed additional π-stacking interactions with Y326$^{7.42}$ and W293$^{6.48}$ that **2** did not possess; therefore, these K233A, Y147A, and W318G mutations affected **2** to a much greater degree than they did to **1** and **6**.

Mutations of Y128$^{2.64}$, V236$^{5.43}$, W293$^{6.48}$, I296$^{6.51}$, H297$^{6.52}$, K303$^{6.58}$, and I322$^{7.38}$ to alanine produced a loss in predicted binding affinities for both **2** and **6**, but not for **1** (**Table S5**). These

mutations resulted in a small loss or gain of predicted binding affinity of **1**. Meanwhile, mutations of I144$^{3.27}$ and Y326$^{7.42}$ to alanine resulted in a loss in predicted binding affinities for all three compounds (**Table S5**).

Overall, **1** exhibited a hydrogen bonding interaction with D147$^{3.32}$ in MOR (the conserved aspartic acid residue within all aminergic GPCRs) while **2** and **6** did not. Compounds **2** and **6** possessed additional hydrogen bonding and hydrophobic interactions with other residues, such as Y148$^{3.33}$, K233$^{5.58}$, and W318$^{7.35}$ (for **2**), and K233$^{5.58}$, W318$^{7.35}$, Y326$^{7.42}$, and W293$^{6.48}$ (for **6**). These additional interactions are likely responsible for the higher binding affinities of **2** and **6** to MOR, compared to that of **1**.

Insights into binding to DOR:
A previous study has suggested that the conserved aspartic acid residue D128$^{3.32}$ in DOR contributed to the stabilization of the ligands, but it was not required for their selectivities to the receptor.[54] Similar to those for KOR and MOR, our docking studies on DOR indicated D128$^{3.32}$ exhibiting hydrogen bonding interaction with the C1-hydroxyl of **1** (**Figure S5B**). Meanwhile, compounds **2** and **6** displayed hydrogen bonding interaction with K108$^{2.63}$, whereas **1** did not (**Figures S5C–D**). We then completed computational site-directed mutagenesis studies on DOR (as we did on KOR and MOR) with these salvinorin-based antagonists to identify the residues that are important for the selectivity and functionality of the ligands to this receptor (**Tables S6–7**).

Previous *in vitro* mutagenesis studies have indicated K108$^{2.63}$, F222$^{5.47}$, W274$^{6.48}$, and Y308$^{7.42}$ were important for the binding of ligands to DOR.[42] Our computational mutagenesis studies indicated that a K108A mutation would lead to a loss of the original binding modes of **2** and **6** (**Table S7**), which suggested that K108 was vital for the binding of these compounds to DOR. While F222$^{5.47}$ displayed no hydrophobic interactions with **1**, **2**, or **6**, we studied its mutation to determine if it contributed to the binding of these compounds to DOR. The results showed that its mutation had minimal effects on the binding of **1**, but produced a loss of the

original binding mode of **2** and a loss in predicted binding affinity of **6**. These results suggested that F222$^{5.47}$ played an important role in the ligand binding to DOR and contributed to the optimal binding of **2** and **6** (**Table S7**).

Compound **1** was observed to exhibit a π-stacking interaction with Y308$^{7.42}$, while **2** and **6** did not; they instead exhibited hydrophobic interactions with this residue (**Figure S5**). A Y308A mutation lowered predicted binding affinities or produce an overall loss of the original binding modes for all three compounds towards DOR (**Table S7**). These results suggested that Y308$^{7.42}$ played a vital role in stabilizing the original binding modes of these compounds in DOR. In addition, mutations of Y109$^{2.64}$, L217$^{5.43}$,

V281$^{6.55}$, L300$^{7.34}$, and I304$^{7.38}$ to alanine resulted in lower predicted binding affinities or loss of the original binding modes for **2** and **6** (but not for **1**) (**Table S7**). These results suggested that Y109$^{2.64}$, L217$^{5.43}$, V281$^{6.55}$, L300$^{7.34}$, and I304$^{7.38}$ contributed to the binding of **2** and **6** to DOR. Notably, **1** also interacted with the aforementioned residues, but their mutations had limited effects on the predicted binding affinity of **1** to DOR. This was probably due to the fact that **1** displayed a different binding mode to DOR than those of **2** and **6** (which were similar to each other) (**Figure S5**). These results suggested that the aforementioned residues aided in, but were not expressly vital to the binding of **1** to DOR.
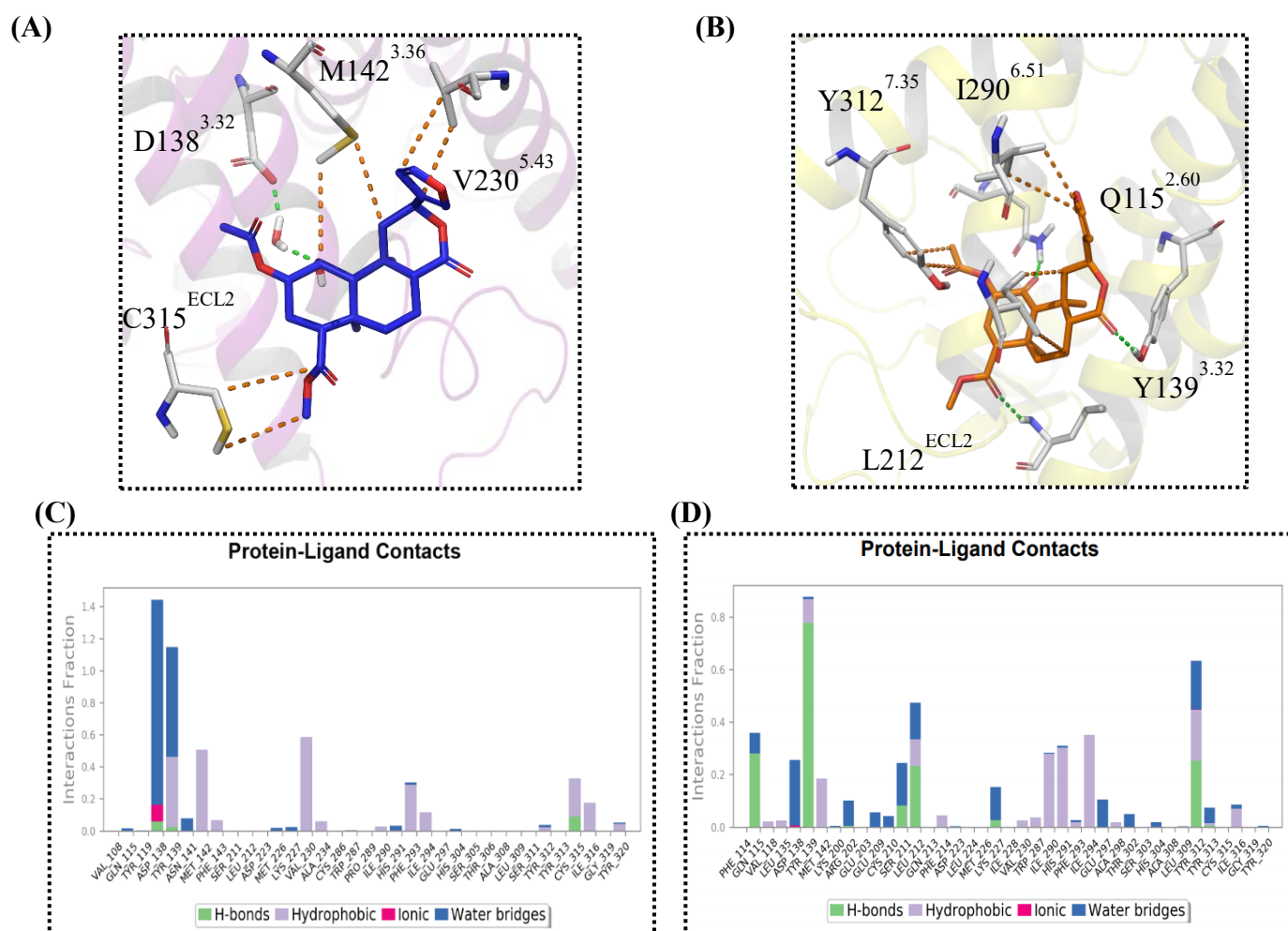

Figure 7. Molecular dynamics simulations' frame snapshot and interaction histogram of compound 1 and salvinorin A within KOR during a 200 ns simulation. **A)** The binding mode of 1 in the inactive state of KOR (PDB: 4DJH); **B)** The binding mode of salvinorin A in the active state of KOR (PDB: 6B73); **C)** Interaction histogram of 1 in the inactive state of KOR; **D)** Interaction histogram of salvinorin A in the active state of KOR. Compound 1 is in blue; salvinorin A is in organge; hydrophobic interactions are denoted as orange dashes, hydrogen bonding interactions are denoted as green dashes, and π-stacking interactions are denoted as blue dashes.
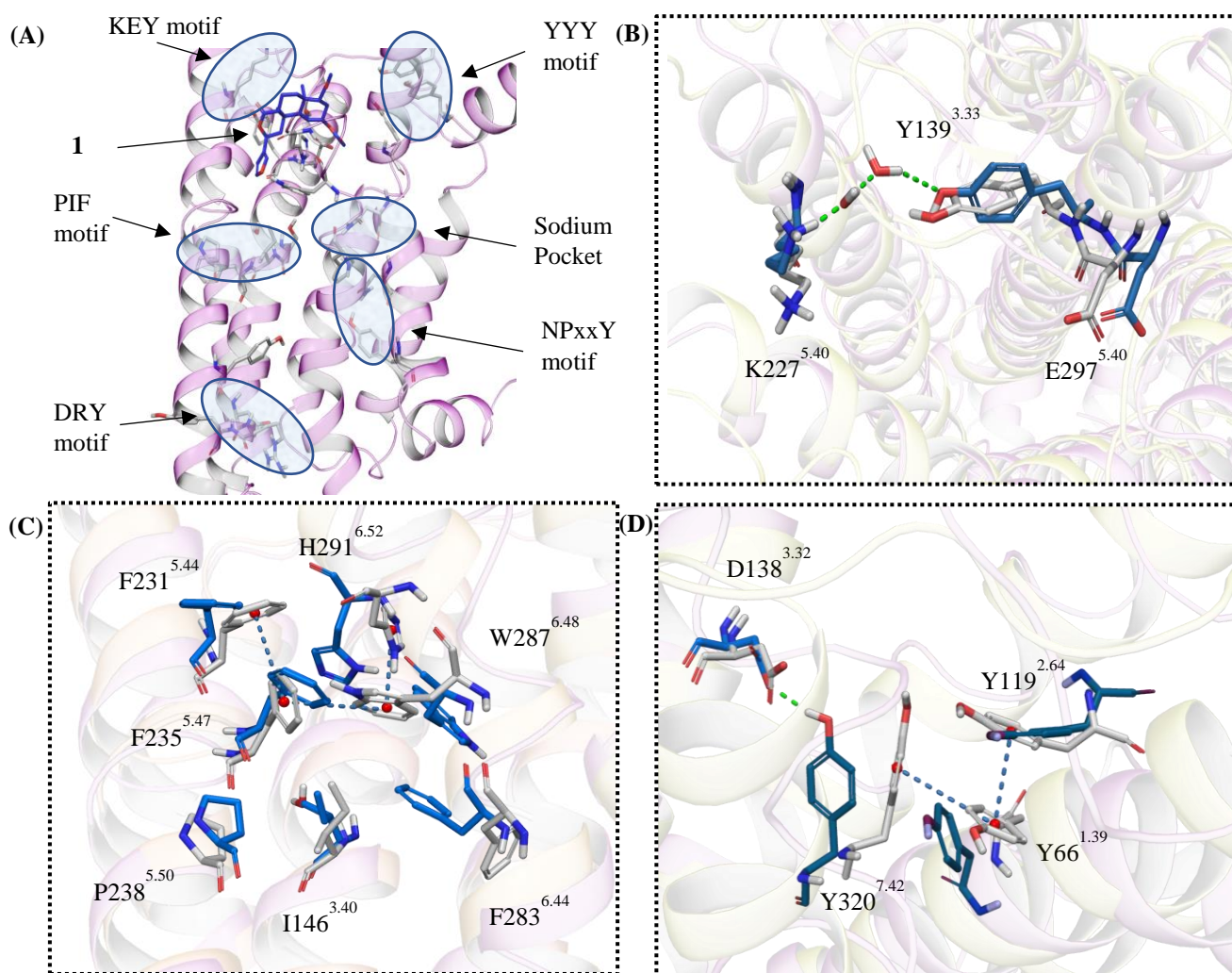
Figure 8. A) Overlay of the transducer regions that are involved in the activation of KOR. Conformational changes between active-state KOR (ball and stick model, blue sticks) and inactive-state KOR (ball and stick model, grey sticks) are highlighted for **(B)** K227$^{5.40}$/E297$^{5.40}$/Y139$^{3.33}$ motif, **(C)** P238$^{5.50}$/I146$^{3.40}$/F283$^{6.44}$ motif and toggle switch residue W287$^{6.48}$, and **(D)** Y66$^{1.39}$/Y119$^{2.64}$/Y320$^{7.42}$/D138$^{3.32}$ putative motif. Hydrogen bonding interactions are denoted as green dashes, and π-stacking interactions denoted as blue dashes. The active-state KOR is in yellow cartoon, and the inactive-state KOR is in purple cartoon.

2.5 Molecular Dynamics Simulations of 1 and Salvinorin A within KOR

We also carried out molecular dynamics (MD) simulations of **1** (an antagonist) and salvinorin A (an agonist) in both the active and inactive states of KOR to further understand their dynamics and the vital interactions for the functionality of the ligands in this receptor. 200 nanosecond MD simulations were carried out using Desmond[56]. The root-mean-square deviation (RMSD) analysis of C-α atoms indicated that KOR reached equilibrium after ~50 ns and remained on a plateau throughout the rest of the 200 ns simulations (**Figure S6**). The RMSD values varied only within a 0.4–1.4 Å range; this clearly indicated that the equilibrium structures of the receptor–ligand complexes were not altered greatly from the starting structures. The RMSD and prime MMGBSA binding free energy data suggested that compound **1** (an antagonist) stably binded to both the active (ΔG = -67.844 ± 5.575 kcal/mol) and inactive states of KOR (ΔG = -59.132 ± 8.091 kcal/mol), with a slight preference

towards the active state. Compound **1** was observed to exhibit interactions with D138[3.32] (water bridge and hydrogen bonding), Y139[3.33] (water bridge and hydrophobic), M142[3.36] (hydrophobic), V230[5.43] (hydrophobic), F293[6.54] (hydrophobic), and C315[7.37] (hydrophobic) within the inactive state of KOR (**Figures 7A** and **7C**).

Our results on the MD simulation of salvinorin A in KOR matched with previously reported results[49] (**Figures 7B** and **7D**). Previous studies on the D138N[3.32] and D138A[3.32] mutations elucidated the important role of D138 in the binding affinity and potency of salvinorin A to KOR, possibly through the removal of an unfavorable desolvation cost.[46] The water-mediated interaction with D138[3.32] in KOR was observed to increase from ~25% in the case of salvinorin A within the active state (with the C1-ketone of salvinorin A, an agonist) to 100% in the case of **1** within the inactive state (with the C1-hydroxyl of **1**, an antagonist). These results suggested that a water-mediated interaction with D138[3.32] in the inactive state may be required for the stabilization of the inactive-state receptor–ligand complex, as seen with the hydrogen bonding interaction between the C1-hydroxyl of the antagonist **1** and D138[3.32] in the inactive state of KOR. On the other hand, limited interaction of salvinorin A with D138[3.32] provides further evidence that the extended hydrogen-bonding network between D138[3.32], water, and salvinorin A are unfavorable, likely due to the overall desolvation cost. Furthermore, these data suggest that the incorporation of a hydrogen-bond donor or removal of the hydrogen-bond acceptor can influence the functionality of salvinorin-based compounds, as seen with compounds **1**, **2**, and **6**.

Interestingly, when we changed the stereochemistry of C1 in **1** (which bears the C1-hydroxyl group) from (*S*) to (*R*), the docking pose of **1** in the inactive state of KOR flipped to maintain the interaction with D138[3.32] (**Figure S7**). This result strengthened the argument that the hydrogen bonding interaction of the correct stereochemistry at C1 with D138[3.32] plays a critical role in maintaining the binding affinity and functionality of salvinorin ligands to KOR.

Previous studies suggested all other aforementioned residues that were important for the binding of the ligands to KOR (see section 2.4) displayed a reduction in the functionality of agonists.[46] Our MD simulations showed limited interactions between these residues and **1** in the inactive state of KOR (**Figure 7C**). These include Y139[3.33] (<1058% interaction within the 200 ns simulation), M142[3.36] (~60%), K227[5.40] (<5%), and H291[6.52] (<5%). Only two of these residues, Y139[3.33] and M142[3.36], interacted 50% or more with **1** in the inactive state of KOR. Notably, while our docking studies suggested good interaction between **1** and K227[5.40] in the inactive state of KOR, our MD simulation indicated limited interaction between them (<5%). Instead, our MD simulation had a significant water-mediated interaction with Y139[3.33] (~100%). Alternatively, within the active-state KOR, compound **1** interacted with the aforementioned residues in an alternative manner: Y139[3.33] (~40%) M142[3.36] (>5%), K227[5.40] (<1%), and H291[6.52] (~55%) (**Figure 9A**).

Unsurprisingly, the interactions are markedly different from one another between states. With this knowledge in hand, we further examined these residues and known motifs that are important for the activation of the KOR. Our results suggested that the lactone–Y139[3.33] interaction between **1** (an antagonist) and KOR may significantly alter the water-bridge normally formed between Y139[3.33] and K227[5.40], thus not allowing for the activation of the receptor (**Figure 8B**). Additionally, H291[6.52] lies near the P238[5.50], I146[3.40], F283[6.44] motif and the rotameric toggle switch residue W287[6.48], two structural features that are known to be important for the activation of the receptor.[57] Interestingly, we found that within the inactive state of KOR (grey sticks), a π-stacking network formed between F231[5.44], F235[5.47], W287[6.48], and H291[6.52], potentially contributing to the stabilization of the inactive state of the receptor (**Figure 8C**). Furthermore, a water molecule was observed to be trapped between the P238[5.50], I146[3.40], and F283[6.44] residues within the inactive state of KOR, but not in the active state of KOR, matching prior mutagenesis and computational studies[46] (**Figure 8C** and **Figure S8**). We also investigated other transducer binding sites that are known to be important for the receptor's activation, including

the sodium pocket, the NPxxY motif, and the DRY motif (**Figure S9**). Overall, these sites showed similar movement upon activation, in the X-ray crystal structure of KOR and selective KOR agonist MP1104[49] (**Figure S9**). Meanwhile, the X-ray crystal structure of KOR and the KOR antagonist JDTiC showed a hydrogen-bonding interaction between T111[2.56] and Y320[7.42] (**Figure S9A**), which was suspected to contribute to the stabilization of the inactive state of the receptor.[49]

Previously, depending on the ligands, Y320[7.42] was observed to form a hydrogen bonding interaction with D138[3.32], which in turn affected the movement of transmembrane helix 7 (TM7) during the activation of KOR. In our studies, Y320[7.42] was seen to form a π-stacking network with Y66[1.39] and Y119[2.64] within the inactive-state KOR–compound **1** complex (**Figure 8D**).
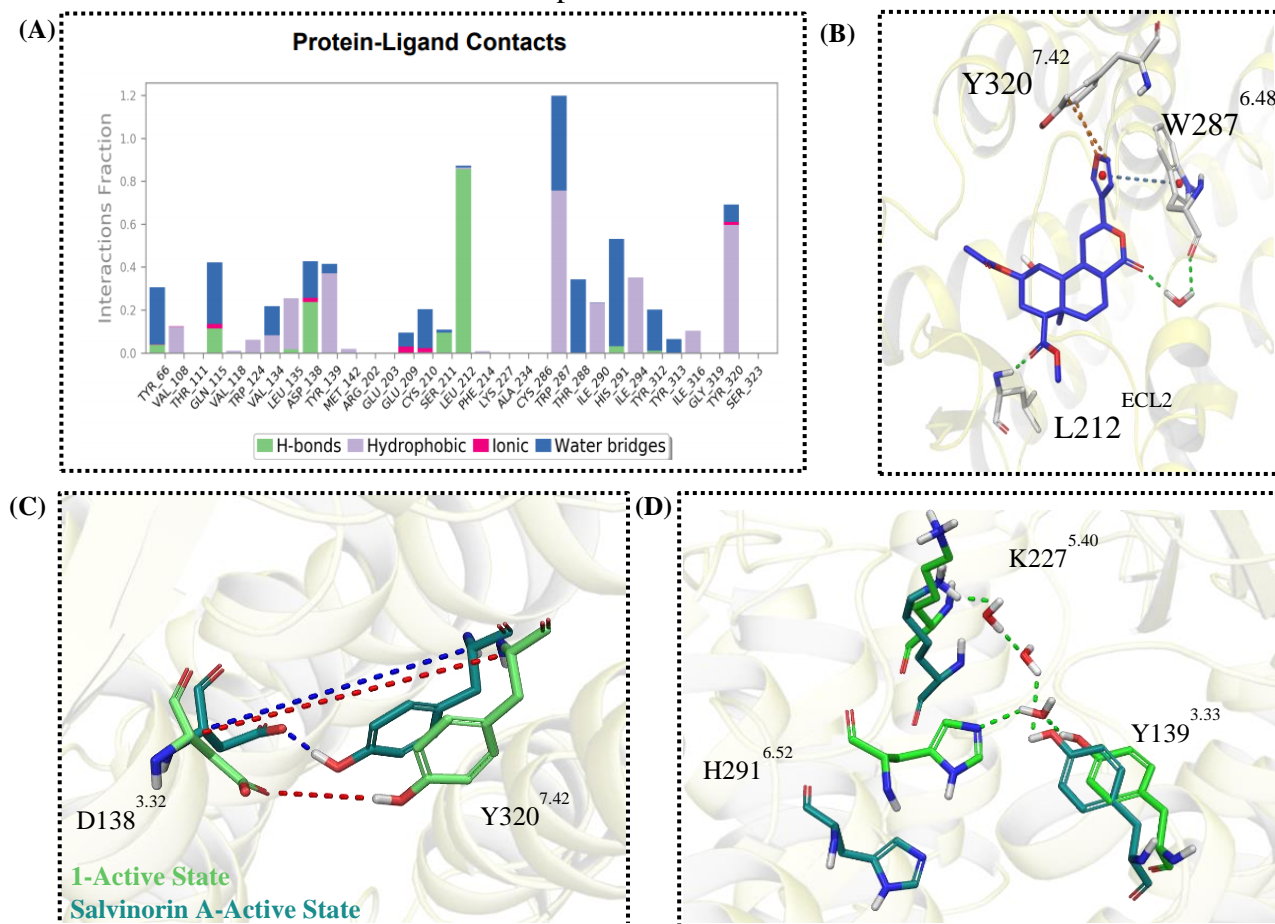

Figure 9. A) Interaction histogram of compound **1** in the active state of KOR. Overlay to show conformational differences between active KOR–compound **1** complex (ball and stick model, light green sticks) and active KOR–salvinoin A complex (ball and stick model, dark green sticks) for (**B**) Y320[7.42]/D138[3.32] region and (**C**) Y139[3.33]/K227[5.40]/H291[6.52] motif.

Meanwhile, Y320[7.42] formed a hydrogen bonding interaction with D138[3.32] in the active-state KOR–salvinorin A complex (**Figure 9B**). Furthermore, our MD simulation of compound **1** (an antagonist) in the active state of KOR showed extensive contacts with Q115[2.60] (water bridge/hydrogen bonding), D138[3.32] (water mediated/H-bond),

Y139[3.33] (hydrophobic/water bridge), L212[ECL2] (H-bond), W287[6.48] (hydrophobic/water-bridge), I290[6.51] (hydrophobic), H291[6.52] (water bridge), I294[6.55] (hydrophobic) and Y320[7.42] (hydrophobic/water bridge) (**Figure 9A**). Interestingly, compound **1** also exhibited a high incidence of water-mediated interaction, but

within the active state of KOR, it predominantly formed hydrogen bonding interaction with D138$^{3.32}$ (**Figure 9A**). Compound **1** also exhibited extensive hydrophobic interactions with Y320$^{7.42}$ (**Figure 9A**). The distances between D138$^{3.32}$ and Y320$^{7.42}$ (from the C=O in D138$^{3.32}$ to the OH in Y320$^{7.42}$), within the active-state KOR–compound **1** and the active-state KOR–salvinorin A complexes, were found to be 4.5 Å and 1.5 Å, respectively (**Figure 9B**). Since the interaction between D138$^{3.32}$ and Y320$^{7.42}$ contributes to the stability of the active-state KOR, the cooperativity of the interactions between different parts of **1** and those aforementioned residues likely disrupted this interaction between D138$^{3.32}$ and Y320$^{7.42}$, thus destabilizing the active state of KOR and contributing to the antagonistic functionality of **1** (**Figure 9B**). Compound **1** also interacted with Y139$^{3.33}$, predominantly through a hydrophobic interaction (**Figure 9A**), while salvinorin A exhibited extensive hydrogen bonding with the ring C lactone. Our MD simulation suggested that compound **1** may have altered the position of K227$^{5.40}$ and allowed Y139$^{3.33}$ to form a water-mediated interaction with H291$^{6.52}$ (**Figure 9C**). We recognize that our MD simulations were only 200 ns, thus may not be long enough to capture all the structural movements leading to the deactivation of KOR, but our studies strongly suggested that all of the aforementioned interactions contributed to the deactivation of the receptor. Furthermore, the data suggested that while D138$^{3.32}$ may not directly affect the binding or functionality of the ligands, this residue provided an anchor point for both compound **1** (an antagonist) and salvinorin A (an agonist) to bind to within the inactive state and the active state of KOR, respectively. The subsequent interactions that occurred as the result of the compound binding then greatly affected the stabilization of the compound–receptor complexes. Altogether, our studies suggested that compound **1** possessed improved interactions with D$^{3.32}$ compared to those of salvinorin A, and disrupted the interaction between the residues that are involved in receptor activation (Y139$^{3.33}$ and K227$^{5.40}$, D138$^{3.32}$ and Y320$^{7.42}$, and M142$^{3.36}$ and H291$^{6.52}$), thus destabilizing the active-state KOR. Furthermore, the transducer regions were observed to have significant differences between the inactive and active states of KOR. These differences matched with those in previous reports on the X-ray crystallography, molecular dynamics, and molecular dynamics studies of KOR.[49] For the first time, we reported a π-stacking network that occurred between Y66$^{1.39}$, Y119$^{2.64}$, and Y320$^{7.42}$ in response to the binding of compound **1** within the inactive state of KOR. Our studies also indicated that this YYY motif may aid in the stabilization of the inactive state of KOR through the prevention of specific intrahelical interactions that were known to be important for signal transduction and receptor activation

3. CONCLUSION

We have reported, for the first time, pharmacokinetic and *in vivo* studies of a salvinorin-based antagonist. Administration of the KOR antagonist **1** reduced spontaneous cocaine-withdrawal behaviors, comparable to nor-BNI. Moreover, **1** produced anti-anxiety-like behavior in the light-dark transition test that was not observed with nor-BNI. The pharmacokinetic profile of **1** is promising with accumulation in the central compartment evidenced after systemic administration. Unlike nor-BNI, **1** appeared to be a short-acting compound (average half-life ($t_{1/2}$) = 3.75 h) with an ideal $t_{1/2}$ in the brain (5.2 h, indicative of full elimination within ~26 h which is consistent with once-daily dosing). T_{max} (the time to maximum concentration) occurred at 30 min in the brain, spinal cord, and plasma, and at 60 min in the liver. These results support the notion that KOR modulation via selective, short-acting antagonism may reduce psychostimulant withdrawal and the associated negative affective symptoms that can contribute to relapse. As such, this class of compounds may hold promise for the improvement of recovery outcomes. In addition, we also carried out in-depth computational studies, including induced-fit docking, computational mutagenesis, and molecular dynamics simulations, to gain insights into why compound **1** acts as an antagonist to KOR, as well as its selectivity towards KOR. Our computational modeling studies indicated this compound binds the KOR, MOR, and DOR through a conserved interaction with the C1-OH-D$^{3.32}$ hydrogen bonding or water-

mediated interaction, likely anchoring the compound in its putative binding mode. As a result, interactions with previously identified residues important for function and affinity to the KOR occur. Our MD simulations revealed compound **1** fit well in the orthosteric pocket of KOR. In particular, **1** displayed strong interactions with the key residues D138$^{3.32}$, Y139$^{3.33}$, M142$^{3.36}$, and V230$^{5.43}$. Compound **1** also stabilized specific motifs known to aid in receptor activation *via* π-stacking (YYY and PIF motif), hydrogen bonding (KEY and DRY motif), or water-mediated interactions (NPxxY motif) within the compound **1**–inactive-state KOR complex. Compound **1** also caused significant changes to the aforementioned motifs in the **1**–active state KOR complex. In terms of drug discovery, the data suggested that incorporation of a hydrogen bond donor (compound **1**) or removal of the hydrogen bond acceptor (compounds **2** and **6**) can influence the functionality of salvinorin-based compounds. Thus, alteration at C1 and C10, and/or concurrent modification at C2, could provide a novel strategy for the future design and development of selective short-acting KOR antagonists.

4. MATERIALS AND METHODS

4.1 Synthesis of 1

Salvinorin A was purchased from Apple Pharms Ingredients Inc. (Bakersville, NC). All other chemicals were purchased from Sigma-Aldrich or Fisher Scientific and used as received unless specified. All syntheses were conducted under anhydrous conditions under an atmosphere of argon, using flame-dried glassware and employing standard techniques for handling air-sensitive materials unless otherwise noted. All solvents were distilled and stored under an argon or nitrogen atmosphere before use. ^{1}H NMR and ^{13}C NMR spectra were recorded on a Bruker-400 and or a Bruker-500 using CDCl$_3$ as the solvent. Chemical shifts (δ) were recorded in parts per million and referenced to CDCl$_3$ (7.24 ppm for ^{1}H NMR and 77.23 ppm for ^{13}C NMR). Coupling constants (J) are in Hz. The following abbreviations were used to designate the multiplicities: s = singlet, d = doublet, t = triplet, q

= quartet, quint = quintet, m = multiplet, br = broad. Melting points were measured using an OptiMelt automated melting point system. LC-MS were measured using an ACQUITY-Waters micromass (ESCi) system. High-resolution mass spectra (HRMS) were measured using a Waters Synapt XS HRMS. Compound **1** was purified via column chromatography (1:2, ethyl acetate:hexanes) and further by HPLC if necessary (7.8×30 mm, 7 μm, C18, gradient water in acetonitrile, flow rate 2 mL/min) until their purities were higher than 95% before being evaluated in *in vitro* and *in vivo* assays; purities were measured using a Waters 2695 analytical HPLC system.

Methyl (2S,4aR,6aR,7R,9S,10R,10aS,10bR)-2-(furan-3-yl)-9,10-dihydroxy-6a,10b-dimethyl-4-oxododecahydro-2H-benzo[f]isochromene-7-carboxylate, 7a.

Salvinorin A (21.6 mg, 0.05 mmol, 1 eq) was dissoved in 4 mL of ethanol and added NaBH$_4$ (9.5 mg, 0.25 mmol, 5 eq) at room temperature. The solution was then heated and stirred at 40 ^{o}C for 1 hour. Upon completion of the reaction as determined via TLC, the solution was cooled to 0°C and acidified to a pH of 3–4. The mixture was then diluted with water (10 mL), extracted with ethyl acetate (3 x 10 mL), washed with brine (10 mL), dried with sodium sulfate, and dried *in vacuo*. The crude was separated via column chromatography (2:1 ethyl acetate:hexanes) to yield **7a** (57%) and **7b** (40%).

^{1}H NMR (400 MHz, CDCl$_3$) δ 7.49 – 7.42 (m, 2H), 6.43 (dd, J = 1.9, 0.9 Hz, 1H), 5.59 (dd, J = 11.5, 5.4 Hz, 1H), 4.23 (s, 1H), 3.70 (s, 3H), 3.64 – 3.58 (m, 1H), 2.50 (dd, J = 13.1, 5.4 Hz, 1H), 2.28 – 2.09 (m, 5H), 1.79 – 1.73 (m, 3H), 1.65 (d, J = 24.6 Hz, 2H), 1.49 (s, 3H), 1.42 – 1.38 (m, 3H), 0.94 (d, J = 1.8 Hz, 1H).

^{13}C NMR (101 MHz, CDCl$_3$) δ 172.97, 172.09, 143.82, 139.33, 125.79, 108.42, 71.90, 71.80, 68.54, 55.73, 54.92, 52.56, 51.54, 44.23, 40.46, 37.71, 36.61, 28.20, 18.62, 17.76, 16.86.

HRMS: Calc. C$_{21}$H$_{29}$O$_7$, Exact Mass [M+H]: 393.1913, HRMS m/z: 393.1916

Melting Point: 228-232ºC

Purity after HPLC: 94.64%

Methyl (2S,4aS,6aR,7R,9S,10R,10aS,10bR)-2-(furan-3-yl)-9,10-dihydroxy-6a,10b-dimethyl-4-oxododecahydro-2H-benzo[f]isochromene-7-carboxylate, 7b

^{1}H NMR (400 MHz, CDCl$_3$) δ 7.50 (dt, J = 1.6, 0.8 Hz, 1H), 7.44 (t, J = 1.7 Hz, 1H), 6.43 (dd, J = 1.9, 0.9 Hz, 1H), 5.30 (dd, J = 11.9, 1.5 Hz, 1H), 4.08 (d, J = 2.9 Hz, 1H), 3.56 (ddd, J = 11.4, 4.8, 3.2 Hz, 1H), 2.47 (d, J = 4.8 Hz, 1H), 2.28 – 2.11 (m, 5H), 1.96 – 1.86 (m, 3H), 1.72 (d, J = 6.7 Hz, 2H), 1.68 (s, 4H), 1.58 – 1.43 (m, 2H), 1.33 (s, 3H), 0.91 (d, J = 1.6 Hz, 1H).

^{13}C NMR (126 MHz, CDCl$_3$) δ 174.42, 173.20, 143.69, 139.68, 123.92, 108.45, 71.84, 69.84, 69.13, 54.83, 54.14, 51.36, 49.04, 46.39, 36.83, 36.70, 36.68, 28.18, 26.52, 18.03, 17.00.

HRMS: Calc. C$_{21}$H$_{29}$O$_7$, Exact Mass [M+H]: 393.1913, HRMS m/z: 393.1922

Melting Point: 233−235 °C

Purity after HPLC: 96.36%

Methyl (2S,4aR,6aR,7R,9S,10R,10aS,10bR)-9-acetoxy-2-(furan-3-yl)-10-hydroxy-6a,10b-dimethyl-4-oxododecahydro-2H-benzo[f]isochromene-7-carboxylate, 1

The diol **7a** (25mg, 0.06 mmol, 1 eq) was dissolved in 7 mL of dry pyridine, treated with 1 mL of acetic anhydride, and stirred for 5 hours. Upon completion of the reaction as determined via TLC, the reaction was terminated by the addition of 1 mL methanol. The mixture was then poured into ice water (50 mL), its pH was adjusted to ~10 by addition of NH$_4$OH, and it was extracted with CHCl$_3$ (2 x 60 mL). The combined organic layers were washed with 10% HCl and 25 mL of water, dried with sodium sulfate, and evaporated *in vacuo*. The mixture was purified via column chromatography (1:1 ethyl acetate:hexanes) to yield compound **1** in a 91% yield.

^{1}H NMR (500 MHz, CDCl$_3$) δ 7.48 – 7.41 (m, 2H), 6.42 (d, J = 1.9 Hz, 1H), 5.55 (dd, J = 11.4, 5.4 Hz, 1H), 4.70 (ddd, J = 12.1, 4.8, 3.1 Hz, 1H), 4.32 – 4.29 (m, 1H), 3.69 (s, 3H), 2.42 (dd, J = 13.2, 5.4 Hz, 1H), 2.32 (q, J = 12.6 Hz, 1H), 2.21 (dd, J = 13.2, 2.6 Hz, 1H), 2.14 – 2.09 (m, 5H), 1.85 – 1.62 (m, 5H), 1.46 (s, 3H), 1.39 (s, 3H), 1.01 (d, J = 1.8 Hz, 1H).

^{13}C NMR (126 MHz, CDCl3) δ 172.58, 171.95, 169.80, 143.83, 139.41, 125.66, 108.46, 74.47, 71.78, 67.21, 55.62, 54.85, 52.46, 51.57, 44.15, 40.51, 37.75, 36.85, 24.75, 21.15, 18.59, 17.89, 16.77.

HRMS: Calc. C$_{23}$H$_{31}$O$_8$, Exact Mass [M+H]: 435.2019, HRMS m/z: 435.2047

Melting Point: 110-112˚C

Purity After HPLC: 96.24%

4.2 *In vivo* Studies

All procedures were preapproved by the Institutional Animal Care and Use Committee (IACUC) at the University of Mississippi. Experiments were carried out in accordance with ethical guidelines defined by the National Institutes of Health (NIH Publication No. 85-23).

4.2.1 Subjects and Housing

Male, adult, C57BL/6N mice (n = 55) were bred in the vivarium at the University of Mississippi (University, MS, USA). Mice were housed 2–5 per cage and kept in a temperature- and humidity-controlled environment on a 12:12 h light:dark cycle (lights off at 09:00 h) with *ad libitum* access to food and water.

4.2.2 Chemicals

Norbinaltorphimine (nor-BNI) and cocaine hydrochloride were obtained from Sigma-Aldrich (St. Louis, MO, USA) and diluted to concentration in sterile saline (0.9%). **1** was synthesized as described above and diluted to concentration in the vehicle (solutol HS 30% in sterile 0.9% saline).

4.2.3 Pharmacokinetic Assessment of 1

Mice received an i.p. injection of **1** and underwent anesthetized, transcardial perfusion with PBS either 5, 15, 30, 60, 120, or 360 min later

(n=3/time-point) as described.[58] Brain, liver, dorsal spinal cord, and plasma were collected at each time-point as described below.

4.2.3.1 Tissue Collection and Extraction

At each time point, mice were anesthetized using isoflurane (4%). The heart was exposed, an incision was made in the right atrium, and whole blood was collected and kept on wet ice in tubes containing sodium citrate. Following transcardial perfusion with 20 mL PBS, the liver, brain, and dorsal spinal cord were grossly dissected. Immediately after each dissection, tissue wet weights were collected and tissues were snap-frozen on dry ice. Plasma was collected from whole blood via centrifugation (10,000 rpm, 10 min). Tissues were homogenized in an equal volume of PBS. Four mL of hexane was added to plasma (0.4 mL) or tissue homogenates (0.8 mL) which were then vortexed (2 min) and centrifugated (10,000 rpm, 10 min). The supernatant was collected and assessed via UV-HPLC as described below.

4.2.3.2 UV-HPLC analytical systems to quantifying 1 in the biological matrix

A UV-HPLC method was used to quantify **1** in the brain, liver, spinal cord, and plasma. The organic phase was transferred to a clean test tube, evaporated under nitrogen, and reconstituted with 1 mL of acetonitrile. The samples were vortexed for 2 minutes and were filtered through a nylon filter (0.45 μm). The samples were analyzed with the same system as before. Following HPLC separation, the compound **1** peak area was quantitated and calculated by PK solver.[62]

4.2.4 Behavioral Assays

Open Field Test. The open-field test was used to assess motor and exploratory behavior.[63,64] Briefly, mice were placed in a corner of the square Plexiglas box (40 × 40 × 35 cm; Stoelting Co., Wood Dale, IL, USA) and allowed to behave for 5 min. Their mean velocity (meters/sec) and total distance traveled (meters) were used as indices for motor behavior. The frequency and time spent rearing were also assessed as an index of motor/exploratory behavior.

Light-Dark Transition Test. The light-dark transition test was used to assess anxiety-like behavior.[65,66] Briefly, mice were placed in the brightly-lit corner of a square Plexiglas box (40 × 40 × 35 cm; Stoelting Co.) that was divided into two compartments (one brightly lit and one enclosed and dark; 20 × 20 cm ea.). Mice were allowed to explore for 5 min. The latency to enter the dark compartment and the time spent in the light chamber were considered indices of anxiety-like behavior. The number of transitions between compartments was used as an index of motor behavior.

Elevated Plus Maze. The elevated plus-maze was used to assess anxiety-like behavior.[64,67] In brief, a plus-shaped elevated maze (37.5 cm from the floor) consisted of two open and two enclosed arms (61 × 5 cm ea.) connected by a central area (5 × 5 cm; Stoelting Co.). Mice were placed in the central area and allowed to freely explore for 5 min. Shorter latencies to enter the open arms and greater time spent on the open arms were considered indices of anti-anxiety-like behavior. The total number of arm entries was recorded as an index of motor behavior.

Tail Suspension Test. The tail suspension test was carried out as previously described.[66,68] In brief, mice were suspended vertically (18 in. from the floor) with their tails secured by laboratory tape to a horizontal surface. A small clean plastic cup was placed over the tails to prevent tail-climbing. Behavior was video recorded for 6 min (with the initial 2 min discarded for acclimation) and the time spent immobile was scored. Greater immobility time was considered an index of increased depression-like behavior.

Biased Conditioned Place Preference Method. Conditioned place preference (CPP) to cocaine (10 mg/kg, i.p., diluted to concentration in sterile 0.9% saline; Sigma-Aldrich, St. Louis, MO, USA) was assessed in a biased paradigm as previously described.[69,70] Briefly, the behavior was recorded and digitally encoded by an ANY-maze behavioral tracking system (Stoelting Co., Wood Dale, IL, USA). Locomotor behavior was assessed during conditioning days. The CPP apparatus (#64101; Stoelting Co.) consisted of

two black conditioning chambers ($18 \times 20 \times 35$ cm), each visually distinguished by the presence of white circles or horizontal stripes on the chamber walls, as well as ~30 lux difference in ambient lighting. Conditioning chambers were connected by a start box/transition chamber (10×20 cm). On day 1, mice freely explored the apparatus for 15 min to establish an initial chamber preference (no significant side preferences were observed across groups). On days 2 and 3 mice were pretreated with vehicle or **1** (5 mg/kg, i.p.) and underwent one cycle of cocaine-conditioning per day consisting of an i.p. saline injection paired with confinement to the preferred chamber for 30 min, followed 4 h later by an i.p. cocaine (10 mg/kg) injection paired with confinement to the less preferred chamber for 30 min. On day 4, mice freely explored the apparatus in order to assess their final chamber preference. The amount of time that mice spent in the chambers or the start/transition box, as well as the distance traveled, was recorded on each day. CPP was quantified as a difference score: CPP d-score = (time spent in the cocaine-paired chamber) – (time spent in the saline-paired chamber; Paris et al., 2014).

4.2.5 Behavioral Procedure

Mice were administered vehicle or a short series of escalating doses of cocaine over 3 days (5, 10, 20 mg/kg, i.p.; **Figure 4**). This dosing range is demonstrated to produce psychostimulation in mice and sensitization when administered sequentially.[71] After receiving the third and final dose of vehicle or cocaine, mice were administered vehicle, compound **1** (5 mg/kg, i.p.), or nor-BNI (5 mg/kg, i.p.) immediately following the final cocaine dose. Forty-eight hours after cocaine cessation, mice were assessed in a behavioral battery to assess their spontaneous motor behavior (open field) as an index of withdrawal, their anxiety-like behavior (light-dark transition test, elevated plus maze), and their depression-like behavior (tail suspension test). On the day of testing, all mice were habituated to the testing room for 30 min prior to assessment.

4.2.6 Statistical Analyses

Behavioral data were analyzed via separate one-way analyses of variance (ANOVA). Following an effect, group differences were determined via Fisher's Protected Least Significant Difference *post hoc* tests with α corrected for family-wise error. *A priori* comparisons were made between manipulated groups and cocaine-exposed mice administered vehicle. All analyses were considered significant when $p < 0.05$.

4.3 Computational Studies

4.3.1 Ligand Preparation

Two-dimensional (2D) structures of salvinorin-based antagonists **1**, **2**, **6**, and salvinorin A were sketched in the 2D sketcher module of Maestro and energy minimized using the ligprep (REF) protocol of the schrödinger suite 2019-1.[51,72] All calculations unless otherwise mentioned were completed using Optimized Potentials for Liquid Simulations 3e (OPLS3e) force field in the gas phase.[51]

4.3.2 Opioid Receptors and Receptor Grid Generation

X-ray crystal structures of the agonist-bound KOR (PDB:6B73), antagonist-bound KOR (PDB:4DJH), antagonist-bound MOR (PDB:4DKL), and antagonist-bound DOR (PDB:4N6H) were used in the docking studies. Protein structures were prepared using Schrödinger Small Molecule Drug Discovery Suite. All water molecules from the X-ray crystal structures were removed, and mutated residues in X-ray crystal structures were changed back to the wildtype. We added missing side chains and removed any extraneous ligands from the active and inactive-state X-ray crystal structures of the opioid receptors. Grid generation was centered on the co-crystalized ligand within the active or inactive-state X-ray crystal structure and defined a $20x20x20$ Å^3 box around the ligand. The rotatable residues within 3 Å of the ligand were defined and the grid was generated.

4.3.3 Native Docking

The prepared protein complexes of the opioid receptors were used to conduct native docking. The native ligand was docked back into the

protein structure with flexible ligand sampling using Glide SP (Schrödinger 2019-1).[73] The docking results were evaluated through a comparison of the best-docked pose determined by Emodel score and the cocrystallized pose by the root-mean-square deviation (RMSD).

4.3.4. Molecular Docking and Scoring

Standard precision (SP) docking method considering flexible ligand sampling using the Glide[73] software was applied. A total of five distinct binding poses (with RMSD $\geq$ 0.5 Å relative to the other poses) were generated for each ligand whenever possible. Selection of the best pose for each ligand was made based on computed values of Emodel score and GlideScore and thorough visual inspection of the predicted binding modes in which favorable interactions with key residues were considered as reported earlier. [45,53,55,74]

4.3.5. Binding Free Energy Calculations

The Prime Molecular Mechanics/Generalized Born Surface Area (MM-GBSA) method was used to calculate the receptor-ligand binding free energies using Prime energy, molecular mechanics (force fields), and the continuum (implicit) solvation energy function (kcal/mol). [52] These were done using the OPLS3e force field in the gas phase and with consideration of the protein side-chain flexibility that was limited to amino acids within a region of 5 Å around the bound ligand.

4.3.6. Molecular Dynamics Simulations

The MD simulations were carried out using the Desmond module of Schrodinger suite 2019.[75] To further assess the stability of the complexes, Salvinorin A bound inactive state KOR, Salvinorin A bound active-state KOR, **1** bound inactive-state KOR and **1** bound active-state KOR was embedded in a POPC (1-palmitoyl-2-oleoyl-sn-glycero-3-phosphocholine) bilayer and solvated with an 11 Å TIP3P water buffer using the OPLS_2005 (optimized potentials for liquid simulations) force field implemented in Desmond, Schrodinger.[76] The system was neutralized by adding chloride ions as needed and 0.15 M NaCl was added to the system. The system was equilibrated using the previously published protocol.[77–79] In brief, the system was simulated for 1 ns using Brownian dynamics in the NVT ensemble at 10 K with the restraint of 50 kcal/mol on solute heavy atoms. Secondly, a 300 ps simulation was run in the NVT ensemble using the Berendsen thermostat (10 K) while retaining the restraint on solute heavy atoms. Thirdly, a 300 ps simulation was run in the NPT ensemble using the Berendsen thermostat (10 K) and barostat (1 atm) while restraints were retained. Over the next 300 ps, the system was gradually heated to 300 K. A final 5 ns simulation was performed in which all restraints were removed. The NPcT ensemble with a temperature of 300 K and a pressure of 1 bar was applied in all the simulations. The simulation length of the production run was 200 ns. The OPLS_2005 force field parameters were used in all simulations. The long-range electrostatic interactions were calculated using the particle mesh Ewald method. The cutoff radius for Coulomb interactions was 9.0 Å. The Langevin coupling schemes were used for the pressure and temperature controls used for the 200 ns production run. Nonbonded forces were calculated using the RESPA integrator and the trajectories were saved at 13.3 ps intervals for analysis. The dynamical behavior and interactions between the ligand and protein were analyzed using the Simulation Interaction Diagram tool implemented in the Desmond MD package. The stability of the MD simulations was monitored by looking at the RMSD of the ligand and protein atom positions in time and by RMSF. Following MD simulations of the complexes, the binding free energies of 1 and Salvinorin A were computed on frames extracted from the trajectory at an interval of 4 ns using the thermal_mmgbsa script by Schrodinger.

ASSOCIATED CONTENT

Supporting Information

The Supporting Information is available free of charge at: https://pubs.acs.org/

AUTHOR INFORMATION

Corresponding Author

* hle@olemiss.edu

AUTHOR CONTRIBUTIONS

CONFLICT OF INTEREST

ACKNOWLEDGMENT

REFERENCES

(1)   Fisher, G.; Roget, N. National Survey on Drug Use and Health. In *Encyclopedia of Substance Abuse Prevention, Treatment, & Recovery*; 2014.

(2)   Kampman, K. M. The Treatment of Cocaine Use Disorder. *Sci. Adv.* **2019**, *5* (10), eaax1532.

(3)   DrugFacts: Cocaine | National Institute on Drug Abuse (NIDA) https://www.drugabuse.gov/publications/drugfacts/cocaine (accessed Feb 13, 2020).

(4)   Kariisa, M.; Scholl, L.; Wilson, N.; Seth, P.; Hoots, B. Drug Overdose Deaths Involving Cocaine and Psychostimulants with Abuse Potential — United States, 2003–2017. *MMWR. Morb. Mortal. Wkly. Rep.* **2019**, *68* (17), 388–395.

(5)   CDC. Other Drugs - Drug Overdose https://www.cdc.gov/drugoverdose/deaths/other-drugs.html (accessed Feb 24, 2022).

(6)   *Substance Abuse and Mental Health Services Administration. Results from the 2020 National Survey on Drug Use and Health: Detailed Tables: Prevalence Estimates, Standard Errors, and Sample Sizes*; 2021.

(7)   Naltrexone & Its Side Effects - Treating Opiate & Alcohol Addiction https://americanaddictioncenters.org/addiction-medications/naltrexone (accessed Feb 13, 2020).

(8)   Methadone Addiction and Abuse - Understanding a Methadone Addiction https://www.addictioncenter.com/opiates/methadone/ (accessed Feb 13, 2020).

(9)   Is buprenorphine addictive? https://www.naabt.org/faq_answers.cfm?ID=33 (accessed Feb 13, 2020).

(10)   DrugFacts: Methamphetamine | National Institute on Drug Abuse (NIDA) https://www.drugabuse.gov/publications/drugfacts/methamphetamine (accessed Jun 27, 2020).

(11)   DrugFacts: Cocaine | National Institute on Drug Abuse (NIDA) https://www.drugabuse.gov/publications/drugfacts/cocaine (accessed Jun 27, 2020).

(12)   Karila, L.; Weinstein, A.; Aubin, H.-J.; Benyamina, A.; Reynaud, M.; Batki, S. L. Pharmacological Approaches to Methamphetamine Dependence: A Focused Review. *Br. J. Clin. Pharmacol.* **2010**, *69* (6), 578–592.

(13)   Rasmussen, K.; White, D. A.; Acri, J. B. NIDA's Medication Development Priorities

in Response to the Opioid Crisis: Ten Most Wanted. *Neuropsychopharmacology* **2019**, *44* (4), 657–659.

(14) Lalanne, L.; Ayranci, G.; Kieffer, B. L.; Lutz, P.-E. The Kappa Opioid Receptor: From Addiction to Depression, and Back. *Front. Psychiatry* **2014**, *5* (DEC), 170.

(15) Carlezon, W. A.; Krystal, A. D. Kappa-Opioid Antagonists for Psychiatric Disorders: From Bench to Clinical Trials. *Depress. Anxiety* **2016**, *33* (10), 895–906.

(16) Wee, S.; Koob, G. F. The Role of the Dynorphin–κ Opioid System in the Reinforcing Effects of Drugs of Abuse. *Psychopharmacology (Berl).* **2010**, *210* (2), 121–135.

(17) Gerra, G.; Fantoma, A.; Zaimovic, A. Naltrexone and Buprenorphine Combination in the Treatment of Opioid Dependence. *J. Psychopharmacol.* **2006**, *20* (6), 806–814.

(18) Graziane, N. M.; Polter, A. M.; Briand, L. A.; Pierce, R. C.; Kauer, J. A. Kappa Opioid Receptors Regulate Stress-Induced Cocaine Seeking and Synaptic Plasticity. *Neuron* **2013**, *77* (5), 942–954.

(19) Marchette, R. C. N.; Gregory-Flores, A.; Tunstall, B. J.; Carlson, E. R.; Jackson, S. N.; Sulima, A.; Rice, K. C.; Koob, G. F.; Vendruscolo, L. F. κ-Opioid Receptor Antagonism Reverses Heroin Withdrawal-Induced Hyperalgesia in Male and Female Rats. *Neurobiol. Stress* **2021**, *14*, 100325.

(20) Munro, T. A.; Berry, L. M.; Van't Veer, A.; Béguin, C.; Carroll, F. I.; Zhao, Z.; Carlezon, W. A.; Cohen, B. M. Long-Acting κ Opioid Antagonists nor-BNI, GNTI and JDTic: Pharmacokinetics in Mice and Lipophilicity. *BMC Pharmacol.* **2012**, *12* (1), 5.

(21) Endoh, T.; Matsuura, H.; Tanaka, C.; Nagase, H. Nor-Binaltorphimine: A Potent and Selective Kappa-Opioid Receptor Antagonist with Long-Lasting Activity in Vivo. *Arch. Int. Pharmacodyn. Ther.* **1992**, *316*, 30–42.

(22) Urbano, M.; Guerrero, M.; Rosen, H.; Roberts, E. Antagonists of the Kappa Opioid Receptor. *Bioorg. Med. Chem. Lett.* **2014**, *24* (9), 2021–2032.

(23) Buda, J. J.; Carroll, F. I.; Kosten, T. R.; Swearingen, D.; Walters, B. B. A Double-Blind, Placebo-Controlled Trial to Evaluate the Safety, Tolerability, and Pharmacokinetics of Single, Escalating Oral Doses of JDTic. *Neuropsychopharmacology* **2015**, *40* (9), 2059–2065.

(24) Metcalf, M. D.; Coop, A. Kappa Opioid Antagonists: Past Successes and Future Prospects. *AAPS J.* **2005**, *7* (3), E704–E722.

(25) Domi, E.; Barbier, E.; Augier, E.; Augier, G.; Gehlert, D.; Barchiesi, R.; Thorsell, A.; Holm, L.; Heilig, M. Preclinical Evaluation of the Kappa-Opioid Receptor Antagonist CERC-501 as a Candidate Therapeutic for Alcohol Use Disorders. *Neuropsychopharmacology* **2018**, *43* (9), 1805–1812.

(26) Proof-of-Concept Trial of CERC-501 Augmentation of Antidepressant Therapy in Treatment-Resistant Depression (RAPID KOR) https://clinicaltrials.gov/ct2/show/NCT019 13535 (accessed Jun 17, 2020).

(27) Hernández-Bello, R.; García-Rodríguez, R. V.; García-Sosa, K.; Peña-Rodríguez, L. M.; Vázquez-Hernández, M.; Ramos-Morales, F. R.; Corcoran, O.; Sánchez-Medina, A. Salvinorin A Content in Legal High Products of Salvia Divinorum Sold in Mexico. *Forensic Sci. Int.* **2015**, *249*, 197–201.

(28) atai Launches Revixia Life Sciences to Develop Salvinorin A for a Variety of Mental Health Conditions https://ir.atai.life/news-releases/news-release-details/atai-launches-revixia-life-sciences-develop-salvinorin-variety
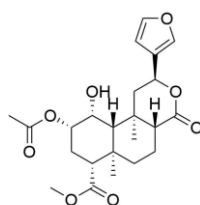
(accessed Feb 28, 2022).

(29) Roach, J. J.; Shenvi, R. A. A Review of Salvinorin Analogs and Their Kappa-Opioid Receptor Activity. *Bioorg. Med. Chem. Lett.* **2018**, *28* (9), 1436–1445.

(30) Beguin, C.; Richards, M. R.; Wang, Y.; Chen, Y.; Liu-Chen, L.-Y.; Ma, Z.; Lee, D. Y. W.; Carlezon, W. A.; Cohen, B. M. Synthesis and in Vitro Pharmacological Evaluation of Salvinorin A Analogues Modified at C(2). *Bioorg. Med. Chem. Lett.* **2005**, *15* (11), 2761–2765.

(31) Akins, N.; Mishra, N.; Harris, H.; Dudhipala, N.; Kim, S. J.; Keasling, A.; Majumdar, S.; Zjawiony, J.; Paris, J.; Ashpole, N.; Le, H. 6,5-Fused Ring, C2-Salvinorin Ester, Dual Kappa and Mu Opioid Receptor Agonists as Analgesics Devoid of Anxiogenic Effects. *ChemMedChem* **2022**, doi: 10.1002/cmdc.202100684.

(32) Beguin, C.; Richards, M. R.; Li, J.-G.; Wang, Y.; Xu, W.; Liu-Chen, L.-Y.; Carlezon, W. A.; Cohen, B. M. Synthesis and in Vitro Evaluation of Salvinorin A Analogues: Effect of Configuration at C(2) and Substitution at C(18). *Bioorg. Med. Chem. Lett.* **2006**, *16* (17), 4679–4685.

(33) Beguin, C.; Potter, D. N.; DiNieri, J. A.; Munro, T. A.; Richards, M. R.; Paine, T. A.; Berry, L.; Zhao, Z.; Roth, B. L.; Xu, W.; Liu-Chen, L.-Y.; Carlezon, W. A.; Cohen, B. M. N-Methylacetamide Analog of Salvinorin A: A Highly Potent and Selective -Opioid Receptor Agonist with Oral Efficacy. *J. Pharmacol. Exp. Ther.* **2007**, *324* (1), 188–195.

(34) Prevatt-Smith, K. M.; Lovell, K. M.; Simpson, D. S.; Day, V. W.; Douglas, J. T.; Bosch, P.; Dersch, C. M.; Rothman, R. B.; Kivell, B.; Prisinzano, T. E. Potential Drug Abuse Therapeutics Derived from the Hallucinogenic Natural Product Salvinorin A. *Medchemcomm* **2011**, *2* (12), 1217.

(35) Munro, T. A.; Duncan, K. K.; Xu, W.; Wang, Y.; Liu-Chen, L.-Y.; Carlezon Jr., W. A.; Cohen, B. M.; Béguin, C. Standard Protecting Groups Create Potent and Selective κ Opioids: Salvinorin B Alkoxymethyl Ethers. *Bioorg. Med. Chem.* **2008**, *16* (3), 1279–1286.

(36) Sałaga, M.; Polepally, P. R.; Sobczak, M.; Grzywacz, D.; Kamysz, W.; Sibaev, A.; Storr, M.; Do Rego, J. C.; Zjawiony, J. K.; Fichna, J. Novel Orally Available Salvinorin A Analog PR-38 Inhibits Gastrointestinal Motility and Reduces Abdominal Pain in Mouse Models Mimicking Irritable Bowel Syndrome. *J. Pharmacol. Exp. Ther.* **2014**, *350* (1), 69–78.

(37) Keasling, A. W.; Pandey, P.; Doerksen, R. J.; Pedrino, G. R.; Costa, E. A.; da Cunha, L. C.; Zjawiony, J. K.; Fajemiroye, J. O. Salvindolin Elicits Opioid System-Mediated Antinociceptive and Antidepressant-like Activities. *J. Psychopharmacol.* **2019**, *33* (7), 865–881.

(38) Lovell, K. M.; Vasiljevik, T.; Araya, J. J.; Lozama, A.; Prevatt-Smith, K. M.; Day, V. W.; Dersch, C. M.; Rothman, R. B.; Butelman, E. R.; Kreek, M. J.; Prisinzano, T. E. Semisynthetic Neoclerodanes as Kappa Opioid Receptor Probes. *Bioorg. Med. Chem.* **2012**, *20* (9), 3100–3110.

(39) Holden, K. G.; Tidgewell, K.; Marquam, A.; Rothman, R. B.; Navarro, H.; Prisinzano, T. E. Synthetic Studies of Neoclerodane Diterpenes from Salvia Divinorum: Exploration of the 1-Position. *Bioorg. Med. Chem. Lett.* **2007**, *17* (22), 6111–6115.

(40) Valdés, L. J. Salvia Divinorum and the Unique Diterpene Hallucinogen, Salvinorin (Divinorin) A. *J. Psychoactive Drugs* **1994**, *26* (3), 277–283.

(41) Hooker, J. M.; Xu, Y.; Schiffer, W.; Shea, C.; Carter, P.; Fowler, J. S. Pharmacokinetics of the Potent Hallucinogen, Salvinorin A in Primates Parallels the Rapid Onset and Short Duration of Effects in Humans.

Neuroimage **2008**, *41* (3), 1044–1050.

(42) Teksin, Z. S.; Lee, I. J.; Nemieboka, N. N.; Othman, A. A.; Upreti, V. V.; Hassan, H. E.; Syed, S. S.; Prisinzano, T. E.; Eddington, N. D. Evaluation of the Transport, in Vitro Metabolism and Pharmacokinetics of Salvinorin A, a Potent Hallucinogen. *Eur. J. Pharm. Biopharm.* **2009**, *72* (2), 471–477.

(43) Gasparyan, A.; Navarrete, F.; Rodríguez-Arias, M.; Miñarro, J.; Manzanares, J. Cannabidiol Modulates Behavioural and Gene Expression Alterations Induced by Spontaneous Cocaine Withdrawal. *Neurotherapeutics* **2021**, *18* (1), 615–623.

(44) Bennett, K. A.; Tehan, B.; Lebon, G.; Tate, C. G.; Weir, M.; Marshall, F. H.; Langmead, C. J. Pharmacology and Structure of Isolated Conformations of the Adenosine A2A Receptor Define Ligand Efficacys. *Mol. Pharmacol.* **2013**, *83* (5), 949–958.

(45) Befort, K.; Tabbara, L.; Bausch, S.; Chavkin, C.; Evans, C.; Kieffer, B. The Conserved Aspartate Residue in the Third Putative Transmembrane Domain of the Delta-Opioid Receptor Is Not the Anionic Counterpart for Cationic Opiate Binding but Is a Constituent of the Receptor Binding Site. *Mol. Pharmacol.* **1996**, *49* (2).

(46) Vardy, E.; Mosier, P. D.; Frankowski, K. J.; Wu, H.; Katritch, V.; Westkaemper, R. B.; Aubé, J.; Stevens, R. C.; Roth, B. L. Chemotype-Selective Modes of Action of κ-Opioid Receptor Agonists. *J. Biol. Chem.* **2013**, *288* (48), 34470–34483.

(47) Roth, B. L.; Baner, K.; Westkaemper, R.; Siebert, D.; Rice, K. C.; Steinberg, S.; Ernsberger, P.; Rothman, R. B. Salvinorin A: A Potent Naturally Occurring Nonnitrogenous Opioid Selective Agonist. *Proc. Natl. Acad. Sci.* **2002**, *99* (18), 11934–11939.

(48) Wu, H.; Wacker, D.; Mileni, M.; Katritch, V.; Han, G. W.; Vardy, E.; Liu, W.; Thompson, A. A.; Huang, X.-P.; Carroll, F. I.; Mascarella, S. W.; Westkaemper, R. B.; Mosier, P. D.; Roth, B. L.; Cherezov, V.; Stevens, R. C. Structure of the Human κ-Opioid Receptor in Complex with JDTic. *Nature* **2012**, *485* (7398), 327–332.

(49) Che, T.; Majumdar, S.; Zaidi, S. A.; Ondachi, P.; McCorvy, J. D.; Wang, S.; Mosier, P. D.; Uprety, R.; Vardy, E.; Krumm, B. E.; Han, G. W.; Lee, M.-Y.; Pardon, E.; Steyaert, J.; Huang, X.-P.; Strachan, R. T.; Tribo, A. R.; Pasternak, G. W.; Carroll, F. I.; Stevens, R. C.; Cherezov, V.; Katritch, V.; Wacker, D.; Roth, B. L. Structure of the Nanobody-Stabilized Active State of the Kappa Opioid Receptor. *Cell* **2018**, *172* (1–2), 55-67.e15.

(50) Laimer, J.; Hofer, H.; Fritz, M.; Wegenkittl, S.; Lackner, P. MAESTRO - Multi Agent Stability Prediction upon Point Mutations. *BMC Bioinformatics* **2015**, *16* (1), 116.

(51) Schrödinger. Maestro | Schrödinger. *Schrödinger Release 2018-1*. 2018.

(52) Genheden, S.; Ryde, U. The MM/PBSA and MM/GBSA Methods to Estimate Ligand-Binding Affinities. *Expert Opinion on Drug Discovery*. Informa Healthcare May 2015, pp 449–461.

(53) Kaserer, T.; Lantero, A.; Schmidhammer, H.; Spetea, M.; Schuster, D. μ Opioid Receptor: Novel Antagonists and Structural Modeling. *Sci. Rep.* **2016**, *6* (1), 1–15.

(54) Befort, K.; Tabbara, L.; Bausch, S.; Chavkin, C.; Evans, C.; Kieffer, B. The Conserved Aspartate Residue in the Third Putative Transmembrane Domain of the Delta-Opioid Receptor Is Not the Anionic Counterpart for Cationic Opiate Binding but Is a Constituent of the Receptor Binding Site. *Mol. Pharmacol.* **1996**, *49* (2), 216–223.

(55) Mo, Y.; Subramanian, G.; Gao, J.; Ferguson, D. M. Cation-π Interactions: An Energy Decomposition Analysis and Its Implication in δ-Opioid Receptor-Ligand

Binding. *J. Am. Chem. Soc.* **2002**, *124* (17), 4832–4837.

(56) Bowers, K. J.; Chow, E.; Xu, H.; Dror, R. O.; Eastwood, M. P.; Gregersen, B. A.; Klepeis, J. L.; Kolossvary, I.; Moraes, M. A.; Sacerdoti, F. D.; Salmon, J. K.; Shan, Y.; Shaw, D. E. Scalable Algorithms for Molecular Dynamics Simulations on Commodity Clusters. In *Proceedings of the 2006 ACM/IEEE Conference on Supercomputing, SC'06*; ACM Press: New York, New York, USA, 2006; p 84.

(57) Zhou, Q.; Yang, D.; Wu, M.; Guo, Y.; Guo, W.; Zhong, L.; Cai, X.; Dai, A.; Jang, W.; Shakhnovich, E.; Liu, Z. J.; Stevens, R. C.; Lambert, N. A.; Babu, M. M.; Wang, M. W.; Zhao, S. Common Activation Mechanism of Class a GPCRs. *Elife* **2019**, *8*.

(58) Ospanov, M.; Sulochana, S. P.; Paris, J. J.; Rimoldi, J. M.; Ashpole, N.; Walker, L.; Ross, S. A.; Shilabin, A. G.; Ibrahim, M. A. Identification of an Orally Bioavailable, Brain-Penetrant Compound with Selectivity for the Cannabinoid Type 2 Receptor. *Molecules* **2022**, *27* (2), 509.

(59) Kepekci Tekkeli, S. E. Development of an HPLC-UV Method for the Analysis of Drugs Used for Combined Hypertension Therapy in Pharmaceutical Preparations and Human Plasma. *J. Anal. Methods Chem.* **2013**, *2013*.

(60) Leonov, K. A.; Vishenkova, D. A.; Lipskikh, O. I.; Pustovoytov, A. V.; Bakibaev, A. A. Development and Validation of HPLC-UV Method for Quantitation of a New Antithrombotic Drug in Rat Plasma and Its Application to Pharmacokinetic Studies. *J. Chromatogr. B Anal. Technol. Biomed. Life Sci.* **2020**, *1160*, 122382.

(61) Rezazadeh, M.; Emami, J. A Simple and Sensitive HPLC Method for Analysis of Imipramine in Human Plasma with UV Detection and Liquid-Liquid Extraction: Application in Bioequivalence Studies. *Res.*
Pharm. Sci. **2016**, *11* (2), 168–176.

(62) Zhang, Y.; Huo, M.; Zhou, J.; Xie, S. PKSolver: An Add-in Program for Pharmacokinetic and Pharmacodynamic Data Analysis in Microsoft Excel. *Comput. Methods Programs Biomed.* **2010**, *99* (3), 306–314.

(63) Hall, C. S.; Ballachey, E. L. A Study of the Rat's Behavior in a Field: A Contribution to Method in Comparative Psychology. In *University of California Publications in Psychology*; 1932; pp 1–12.

(64) Paris, J. J.; Singh, H. D.; Ganno, M. L.; Jackson, P.; McLaughlin, J. P. Anxiety-like Behavior of Mice Produced by Conditional Central Expression of the HIV-1 Regulatory Protein, Tat. *Psychopharmacology (Berl).* **2014**, *231* (11), 2349–2360.

(65) Bourin, M.; Hascoët, M. The Mouse Light/Dark Box Test. *Eur. J. Pharmacol.* **2003**, *463* (1–3), 55–65.

(66) Salahuddin, M. F.; Qrareya, A. N.; Mahdi, F.; Jackson, D.; Foster, M.; Vujanovic, T.; Box, J. G.; Paris, J. J. Combined HIV-1 Tat and Oxycodone Activate the Hypothalamic-Pituitary-Adrenal and -Gonadal Axes and Promote Psychomotor, Affective, and Cognitive Dysfunction in Female Mice. *Horm. Behav.* **2020**, *119*, 104649.

(67) File, S. E.; Lippa, A. S.; Beer, B.; Lippa, M. T. Animal Tests of Anxiety. *Curr. Protoc. Neurosci.* **2004**, *Chapter 8* (1), Unit 8.3.

(68) Steru, L.; Chermat, R.; Thierry, B.; Simon, P. The Tail Suspension Test: A New Method for Screening Antidepressants in Mice. *Psychopharmacology (Berl).* **1985**, *85* (3), 367–370.

(69) Paris, J. J.; Reilley, K. J.; McLaughlin, J. P. Kappa Opioid Receptor-Mediated Disruption of Novel Object Recognition: Relevance for Psychostimulant Treatment. *J. Addict. Res. Ther.* **2011**, *S4*, 007.

(70) Paris, J. J.; Carey, A. N.; Shay, C. F.; Gomes, S. M.; He, J. J.; McLaughlin, J. P. Effects of Conditional Central Expression of HIV-1 Tat Protein to Potentiate Cocaine-Mediated Psychostimulation and Reward among Male Mice. *Neuropsychopharmacology* **2014**, *39* (2), 380–388.

(71) Uzbay, I. T.; Wallis, C. J.; Lal, H.; Forster, M. J. Effects of NMDA Receptor Blockers on Cocaine-Stimulated Locomotor Activity in Mice. *Behav. Brain Res.* **2000**, *108* (1), 57–61.

(72) Schrödinger. LigPrep. *Schrödinger Release 2020-1: Schrödinger, LLC, New York, NY, 2020*. 2020.

(73) Friesner, R. A.; Banks, J. L.; Murphy, R. B.; Halgren, T. A.; Klicic, J. J.; Mainz, D. T.; Repasky, M. P.; Knoll, E. H.; Shelley, M.; Perry, J. K.; Shaw, D. E.; Francis, P.; Shenkin, P. S. Glide: A New Approach for Rapid, Accurate Docking and Scoring. 1. Method and Assessment of Docking Accuracy. *J. Med. Chem.* **2004**, *47* (7), 1739–1749.

(74) Rasmussen, S. G. F.; Devree, B. T.; Zou, Y.; Kruse, A. C.; Chung, K. Y.; Kobilka, T. S.; Thian, F. S.; Chae, P. S.; Pardon, E.; Calinski, D.; Mathiesen, J. M.; Shah, S. T. A.; Lyons, J. A.; Caffrey, M.; Gellman, S. H.; Steyaert, J.; Skiniotis, G.; Weis, W. I.; Sunahara, R. K.; Kobilka, B. K. Crystal Structure of the β 2 Adrenergic Receptor-Gs Protein Complex. *Nature* **2011**, *477* (7366), 549–557.

(75) Gygi, F.; Draeger, E. W.; Schulz, M.; De Supinski, B. R.; Gunnels, J. A.; Austel, V.; Sexton, J. C.; Franchetti, F.; Kral, S.; Ueberhuber, C. W.; Lorenz, J. Large-Scale Electronic Structure Calculations of High-Z Metals on the BlueGene/L Platform. In *Proceedings of the 2006 ACM/IEEE Conference on Supercomputing, SC'06*; 2006.

(76) Jorgensen, W. L.; Chandrasekhar, J.; Madura, J. D.; Impey, R. W.; Klein, M. L. Comparison of Simple Potential Functions for Simulating Liquid Water. *J. Chem. Phys.* **1983**, *79* (2), 926–935.

(77) Zou, Y.; Wang, X.; Sims, J.; Wang, B.; Pandey, P.; Welsh, C. L.; Stone, R. P.; Avery, M. A.; Doerksen, R. J.; Ferreira, D.; Anklin, C.; Valeriote, F. A.; Kelly, M.; Hamann, M. T. Computationally Assisted Discovery and Assignment of a Highly Strained and PANC-1 Selective Alkaloid from Alaska's Deep Ocean. *J. Am. Chem. Soc.* **2019**, *141* (10), 4338–4344.

(78) Pandey, P.; Roy, K. K.; Doerksen, R. J. Negative Allosteric Modulators of Cannabinoid Receptor 2: Protein Modeling, Binding Site Identification and Molecular Dynamics Simulations in the Presence of an Orthosteric Agonist. *J. Biomol. Struct. Dyn.* **2020**, *38* (1), 32–47.

(79) Stoddard, S. V.; Stoddard, S. D.; Oelkers, B. K.; Fitts, K.; Whalum, K.; Whalum, K.; Hemphill, A. D.; Manikonda, J.; Martinez, L. M.; Riley, E. G.; Roof, C. M.; Sarwar, N.; Thomas, D. M.; Ulmer, E.; Wallace, F. E.; Pandey, P.; Roy, S. Optimization Rules for SARS-CoV-2 Mpro Antivirals: Ensemble Docking and Exploration of the Coronavirus Protease Active Site. *Viruses* **2020**, *12* (9).

TABLE OF CONTENT

1